

AD-A100 507

TEXAS UNIV AT AUSTIN APPLIED RESEARCH LABS  
AN EXPERIMENTAL INVESTIGATION OF A NEYMAN-PEARSON DETECTOR FOR --ETC(U)  
MAR 81 A J ESTES

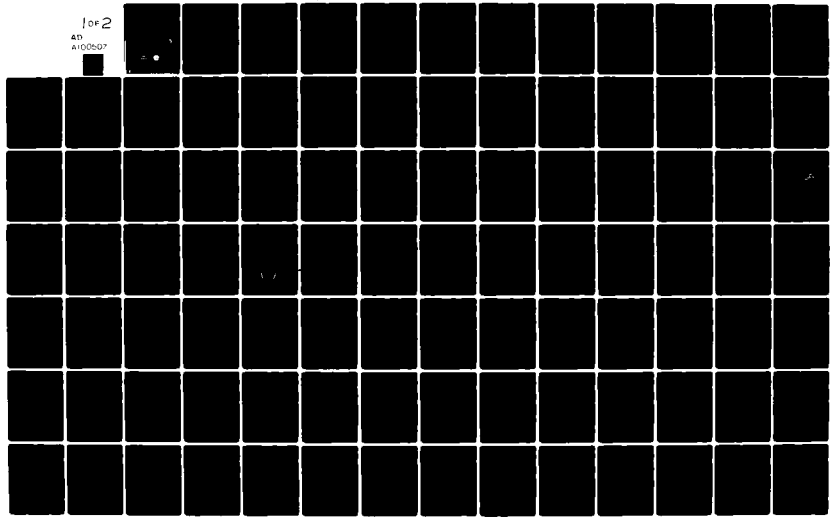
N00014-80-C-0490

NL

UNCLASSIFIED

ARL-TR-81-14

for 2  
AD  
A100007



ADA100507

LEVEL

12

14

ARL-TR-81-14

Copy No. 77

6

AN EXPERIMENTAL INVESTIGATION OF A NEYMAN-PEARSON  
DETECTOR FOR A MULTICHANNEL ACTIVE SONAR OPERATING  
IN A REVERBERANT ENVIRONMENT

10

Arthur J. Estes

APPLIED RESEARCH LABORATORIES  
THE UNIVERSITY OF TEXAS AT AUSTIN  
POST OFFICE BOX 8029, AUSTIN, TEXAS 78712

11

3 March 1981

12

99

9

Technical Report

APPROVED FOR PUBLIC RELEASE;  
DISTRIBUTION UNLIMITED.

DTIC  
RECEIVED  
JUN 23 1981

15

00014-80-C-0490

Prepared for:

OFFICE OF NAVAL RESEARCH  
DEPARTMENT OF THE NAVY  
ARLINGTON, VA 22217

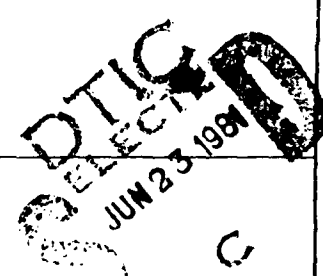


FILE COPY  
404434  
01 6 99 005

## UNCLASSIFIED

SECURITY CLASSIFICATION OF THIS PAGE (When Data Entered)

REPORT DOCUMENTATION PAGE		READ INSTRUCTIONS BEFORE COMPLETING FORM
1. REPORT NUMBER	2. GOVT ACCESSION NO.	3. RECIPIENT'S CATALOG NUMBER
AD-A100 507		
4. TITLE (and Subtitle) AN EXPERIMENTAL INVESTIGATION OF A NEYMAN-PEARSON DETECTOR FOR A MULTICHANNEL ACTIVE SONAR OPERATING IN A REVERBERANT ENVIRONMENT		5. TYPE OF REPORT & PERIOD COVERED technical report
7. AUTHOR(s) Arthur J. Estes		6. PERFORMING ORG. REPORT NUMBER ARL-TR-81-14
9. PERFORMING ORGANIZATION NAME AND ADDRESS Applied Research Laboratories The University of Texas at Austin Austin, Texas 78712		8. CONTRACT OR GRANT NUMBER(s) N00014-80-C-0490
11. CONTROLLING OFFICE NAME AND ADDRESS Office of Naval Research Department of the Navy Arlington, Virginia 22217		10. PROGRAM ELEMENT, PROJECT, TASK AREA & WORK UNIT NUMBERS Item 0004
14. MONITORING AGENCY NAME & ADDRESS(if different from Controlling Office)		12. REPORT DATE 3 March 1981
		13. NUMBER OF PAGES 92
16. DISTRIBUTION STATEMENT (of this Report)		15. SECURITY CLASS. (of this report) UNCLASSIFIED
		15a. DECLASSIFICATION/DOWNGRADING SCHEDULE
Approved for public release; distribution unlimited.		
17. DISTRIBUTION STATEMENT (of the abstract entered in Block 20, if different from Report)		
18. SUPPLEMENTARY NOTES		
19. KEY WORDS (Continue on reverse side if necessary and identify by block number) sonar detection reverberation Neyman-Pearson		
20. ABSTRACT (Continue on reverse side if necessary and identify by block number) This report describes a study in which several aspects of the discrete time Neyman-Pearson detector are investigated using experimental acoustic data. The problem considered is that of detecting a known signal from an active sonar operating in a reverberant environment. The noise background consists of sonar returns obtained by directing a transmitter and receiver toward the wind driven surface of a freshwater lake. Data for the known signal consist of echoes from a styrofoam sphere. Both signal and reverberation returns are digitized outputs from four elements of a linear receiving array. Two types of sonar transmissions		



UNCLASSIFIED

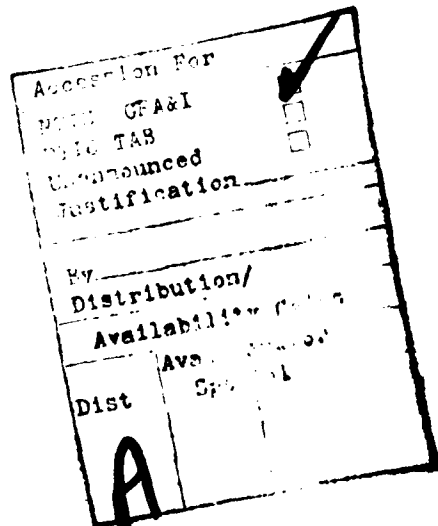
SECURITY CLASSIFICATION OF THIS PAGE(When Data Entered)

20. (cont'd)

employed are 1.0 msec pulsed continuous wave (cw) signal at a carrier frequency of 80 kHz and a 1.0 msec pulsed linear frequency modulated (LFM) signal with a 10 kHz sweep centered at 80 kHz.

Signal-plus-noise events are created by adding digital samples from the styrofoam ball echoes to samples from the reverberation returns at specified signal-to-noise ratios. The reverberation process is assumed to be Gaussian with a known covariance matrix. For the experimental detector evaluation, this matrix is computed by averaging over an ensemble of approximately 100 reverberation events. This matrix is used in the Neyman-Pearson detector to process these same 100 returns. The performance obtained experimentally in this fashion is compared to that predicted from theoretical considerations based on the Gaussian assumption and the covariance matrix. Finally, the performance of the Neyman-Pearson detector is shown for these data to provide the following improvement over a simple matched filter:

- (1) 13 dB for the 1.0 msec cw data, and
- (2) 8 dB for the 1.0 msec LFM data.



UNCLASSIFIED

SECURITY CLASSIFICATION OF THIS PAGE(When Data Entered)

## TABLE OF CONTENTS

	<u>Page</u>
LIST OF FIGURES	7
LIST OF TABLES	vii
I. INTRODUCTION	1
II. THEORY	7
A. Background	7
B. The Neyman-Pearson Lemma	10
C. The Likelihood Ratio Detector	13
1. Assumptions	13
2. Detector Formulation	15
3. Threshold Determination and Performance Prediction	21
D. Sampling Technique	27
III. EXPERIMENTAL PROCEDURE	33
A. Data Acquisition Site and Environmental Conditions	33
B. Description of Transducer Array	36
C. Reverberation Measurement	36
D. Target Echoes	36
E. Data Acquisition	40
IV. EXPERIMENTAL RESULTS	45
A. Alignment of Digital Samples	45
B. Computation of the Covariance Matrix Estimate and Data Segment Selection	46

	<u>Page</u>
C. The Detection Problem	56
D. Analysis of Results	59
1. Effect of Input Signal-to-Noise Ratio	59
2. Effect of Sampling Frequency	62
3. Multiple Channels	65
4. Suboptimum Detectors - Multiple Channels	65
5. Suboptimum Detectors - Single Channel	72
6. Detection Probability versus Signal-to-Noise Ratio	72
V. CONCLUSIONS AND RECOMMENDATIONS	77
APPENDIX	81
REFERENCES	87

## LIST OF FIGURES

<u>Figure No.</u>	<u>Title</u>	<u>Page</u>
2.1	General Detection Problem	8
2.2	Likelihood Ratio Processor	11
2.3	Multichannel Likelihood Ratio Processor	19
2.4	Typical Conditional Probability Densities for the Test Statistic $\lambda$ and Associated Error Probabilities	24
2.5	Predicted Detector Performance with $\sigma_\lambda$ as a Parameter	28
3.1	Location of Lake Travis Test Station	34
3.2	A Front View of the Transducer Array	37
3.3	A Vertical Profile of the Geometric Features of the Reverberation Experiment	38
3.4	Underwater Sound Reflector	39
3.5	A Block Diagram of the Analog Data Recording System	41
3.6	Block Diagram of Digitization Equipment	42
4.1	Envelopes of the Normalized Covariance Matrix	50
4.2	Phases of the Covariance Matrix	51
4.3	Envelopes of the Normalized Covariance Matrix	52
4.4	Phases of the Covariance Matrix	53
4.5	Covariance Between Elements 1 and 2	54
4.6	Covariance Between Elements 1 and 2	55
4.7	Example Envelopes and Phases of Signal + Reverberation	57

<u>Figure No.</u>	<u>Title</u>	<u>Page</u>
4.8	Experimental and Predicted Detector Performance for Various Input Signal-to-Noise Ratios	60
4.9	Experimental and Predicted Detector Performance for Various Input Signal-to-Noise Ratios	61
4.10	Effect of Sampling Parameter k on Detector Performance	63
4.11	Effect of Sampling Parameter k on Detector Performance	64
4.12	Detector Performance with Number of Channels as a Parameter	66
4.13	Detector Performance with Number of Channels as a Parameter	67
4.14	Comparison of Optimum and Suboptimum Detector Performances for a 0.1 False Alarm Rate	74
4.15	Comparison of Optimum and Suboptimum Detector Performances for a 0.1 False Alarm Rate	76

## LIST OF TABLES

<u>Table No.</u>	<u>Title</u>	<u>Page</u>
I	Environmental Factors of Reverberation and Target Echo Experiments	35
II	Comparison of Detector Performance ( $d^2$ ) for Optimum and Simplified Processors	71
III	Comparison of Single Channel Detector Performance ( $d^2$ ) for Optimum and Simplified Processors	73

## I. INTRODUCTION

### A. Background

This study is conducted within the framework of the detection problem encountered in an active sonar employing multiple receiving elements. Active sonar is a device for discovering distant objects such as submarines, ships, fish, etc. It utilizes a transducer which generates acoustic energy of wavelengths on the order of 1 to 20 cm in the form of pulses of large amplitude and brief duration. When this energy strikes a reflecting object it is scattered in all directions. Some of this energy returns to the transducer as signals which are received by the sonar receiver. This study considers the manner in which these signals are processed by the sonar receiver.

At first glance one might think that targets could be detected at any range merely by increasing the amplification of the received signals. In actual sonar conditions, however, there are several types of interference which are detrimental to the sonar receiver's performance. These sources of interference can be classified as system noise, ambient noise, and reverberation noise.

System noise includes both thermal noise produced in the receiver itself and noise produced by the motion of the array through the water. In this study flow noise is not significant since a stationary array is used. Also, the other noise sources are assumed to be the predominant effects which limit the receiver's performance.

Ambient noise sources are often quite powerful and contain a wide range of frequencies. Some examples of this type of noise source are wave action at the surface, meteorological effects, and noise generated

by distant ships. Ambient noise sources are of particular interest to the designer of passive sonars. In this study the ambient noise field is assumed to be negligible as compared to reverberation noise.

Reverberation is the noise source which poses the most difficult problem for an active sonar receiver. Since this noise is caused by the transmitted signal, it has many characteristics similar to the echo from an underwater object. It does no good to increase the gain of the receiver's amplifier because the power of the reverberation is increased proportionately. There are three types of reverberation: volume, bottom, and surface reverberation, and these are caused by reflection of the transmitted signal from irregularities in the body of water and from the lower and upper surfaces of the water respectively.<sup>1</sup> The type of noise considered in this study is surface reverberation.

In active sonar signal detection the target echo is often received at a low level compared to the energy in the surface reverberation. In an attempt to enhance the target signal, some current Navy sonars employ matched filtering to process the received sonar signal. Since this type processing consists of merely correlating the incoming signal with a replica of the transmitted waveform, it is optimum (in the Neyman-Pearson sense) when the noise is a Gaussian process, both independent and stationary. However, surface reverberation is in general a nonstationary process with a finite correlation time; therefore a processor that must cope with surface reverberation must be more complicated. There is an extensive body of literature on theoretical signal processing techniques designed to determine whether or not a target echo is present in a given sonar return. We have some knowledge of more optimum ways to process these signals, but we have no feel for the efficiency of these improved processing techniques. Both a brief theoretical review and some experimental effort seem justified. Specifically, it would be valuable to know how a given signal processing technique performs in the presence of surface reverberation.

## B. Previous Studies

As stated previously, much work has already been done to develop better techniques for processing sonar signals from multiple receiving elements. Mermoz<sup>2</sup> has developed the optimum receiver structure to maximize the output signal-to-noise ratio. In that work, the noise process is assumed stationary with a known correlation matrix, but otherwise arbitrarily distributed. The result is a set of generalized matched filters. Each filter response depends on the signal and the matrix of spectral densities of the noise process. An excellent summary of Mermoz's work is given by Horton.<sup>1</sup>

Middleton and Groginsky<sup>3</sup> specified the receiver structure which is optimum in the Bayes sense, i.e., minimum average cost to the observer. That paper dealt with Gaussian signals in the presence of Gaussian noise, but stationarity was not an assumption. One of the more important results presented was that factorization of the spatial-temporal operations is not, in general, possible in optimum systems. Factorization here is the "separation of the required filter into two successive operations--the first depending only on the geometry of the array, the second depending only on the statistics of the noise process."<sup>3</sup> Current Navy sonars utilize factored processing by first beamforming and then performing some temporal operation such as matched filtering. The optimum detector developed in that paper utilizes a set of time varying filters which are determined by the covariance functions of the noise and signal processes.

In both of these works the covariance functions of the noise process are assumed known. For surface reverberation, the process that is a major limitation of active sonar receivers, this assumption is hardly a minor one. In recent years, however, several experimental studies have been conducted which considered the statistical nature of this process. The papers by Plemons<sup>4</sup> and Plemons, Middleton, and Shooter<sup>5,6</sup> contain experimental results of the temporal and spectral characteristics of the process. Their experiment utilized a single transducer to measure reverberation signals from a lake surface. In a similar manner Frazer<sup>7,8</sup> and

Omichi<sup>9</sup> studied the joint spatial and temporal properties of surface reverberation by analyzing signals from multiple receiving elements. Although these works have contributed significantly to our knowledge of this particular random process, there is still a large gap between current sonar signal processors and the optimal processors mentioned above.

To justify the implementation of more powerful processors, the sonar designer needs to know how much improvement there will be over simpler processors. This is an area where the acoustic signal processing literature is not very abundant. There have been a few such studies, two of which are mentioned here. Hoffman<sup>10,11</sup> presented some theoretical and experimental work implementing a simplified (compared to Middleton's and Groginsky's) Bayesian processor using sonar echoes from several contacts. He used the processor to classify echoes from objects of different sizes and materials. To learn more about the optimum detector's performance, there is a need for experimental evaluation using surface reverberation data.

One such study was performed by Baker and Cunningham<sup>12</sup> using single channel beamformed data from the Navy's AN/SQS-23 sonar. These data included submarine echoes as well as segments of pure surface reverberation. Reverberation and signal ensembles were formed over a hundred consecutive pings and used to compute the signal and noise sample covariance matrices. Signal-plus-noise returns were artificially created by adding a signal return to the reverberation echoes at various signal-to-noise ratios. The signals thus formed were processed with the discrete form of the Bayesian detector specified by Middleton and Groginsky.

#### C. The Present Study

The present study is an experimental evaluation of an optimum detector for a multichannel active sonar operating in the presence of surface reverberation. The detector is optimum in the Neyman-Pearson sense, i.e., the detection probability is maximized for a given false

alarm probability. The design of the detector is based on the assumption of a known signal in Gaussian noise.

Experiments in the open ocean with actual Navy sonars are expensive and present difficulties in controlling many parameters of interest. On the other hand a high degree of experimental control is possible in taking lake data, and lake surface reverberation bears many similarities to that of the ocean. In this study an ensemble of reverberation returns is created by scattering sound from a wind driven surface of a freshwater lake. Signals on each of six receiver elements (5.1 cm center to center) are sampled and digitized. Signal-plus-noise returns are formed in a general purpose computer by adding an experimental target echo to each member of the noise ensemble at various signal-to-noise ratios. The covariance matrix is estimated from the ensemble and employed by the detector. The detector's performance is then analyzed by processing the signal-plus-noise returns.

The detector's performance is presented in the form of receiver operating characteristic (ROC) curves. The aspects of the detector included in this study are:

1. the effect of sampling frequency;
2. the effect of transmit type; transmissions include the following types: a 1.0 msec pulsed continuous wave (cw) signal at a carrier frequency of 80 kHz and a 1.0 msec pulsed linear frequency modulated (LFM) signal with a 10 kHz sweep centered at 80 kHz;
3. the effect of assuming the noise process is stationary over the time duration of the signal;
4. the effect of assuming the noise samples are
  - (1) uncorrelated in space but correlated in time,
  - (2) uncorrelated in time but correlated in space,
  - (3) uncorrelated in both space and time.

## II. THEORY

This section includes a brief theoretical review of the technique used to design the detector being considered. The Neyman-Pearson lemma is presented, without proof, as justification for choosing the likelihood ratio test employed by the detector. Several assumptions are made leading to the detector's implementation and the performance prediction. Finally, the sampling procedure and its relation to the detection problem are described.

### A. Background

In an abstract sense the detection problem is represented by Fig. 2.1. In a sonar system the observation might be a set of samples from transducer element signals over some finite time interval. The observation will be considered as an event which could have been produced by one of two possible causes. The two possible causes considered here are signal plus noise and noise only. The null hypothesis, that noise only was responsible for the event, will be designated as  $H_0$  and the other hypothesis, that the event was caused by signal-plus-noise, by  $H_1$ .

The data processor must take an observation  $x$  and produce a decision as to which hypothesis is most likely. The decision rule will be determined by dividing the observation space into two regions  $R_0$  and  $R_1$  so that for any observation  $x$  either  $H_0$  or  $H_1$  can be chosen as the true case. To arrive at a suitable decision boundary between  $R_0$  and  $R_1$  the four possible outcomes must be considered. The four outcomes are:

- (1) given  $H_1$  is true, the detector decides  $H_1$  (true alarm),
- (2) given  $H_0$  is true, the detector decides  $H_0$  (true dismissal),
- (3) given  $H_0$  is true, the detector decides  $H_1$  (false alarm),
- (4) given  $H_1$  is true, the detector decides  $H_0$  (false dismissal).

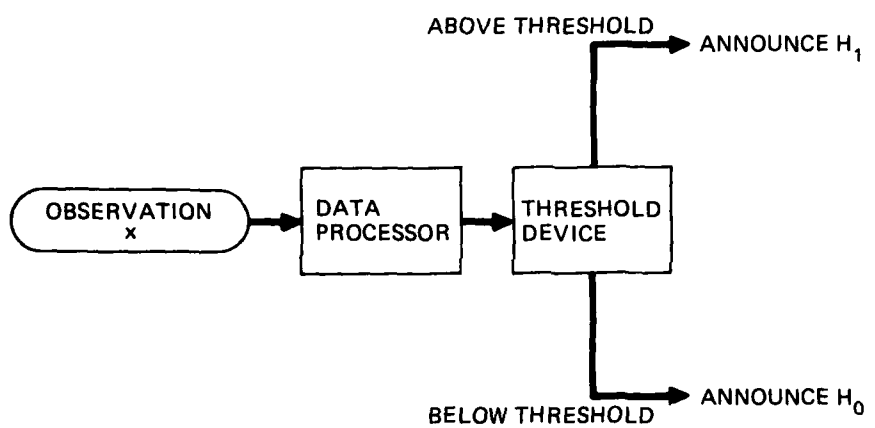


**FIGURE 2.1**  
**GENERAL DETECTION PROBLEM**

ARL:UT  
AS-81-271  
MEF-GA  
3-11-81

If the probability that  $H_0$  or  $H_1$  is true is known a priori and a cost is assigned to each of the four outcomes, then the Bayes criterion can be used to determine a decision rule. This is accomplished by minimizing the expected cost or average risk  $R$ . Let  $\pi_0$  and  $\pi_1$  be the a priori probabilities of  $H_0$  and  $H_1$ , respectively, and  $c_{ij}$  be the cost of announcing  $H_i$  when  $H_j$  is true. Then the average risk  $R$  is

$$\begin{aligned} R = & c_{00} \pi_0 \Pr\{\text{choosing } H_0 | H_0 \text{ is true}\} \\ & + c_{10} \pi_0 \Pr\{\text{choosing } H_1 | H_0 \text{ is true}\} \\ & + c_{11} \pi_1 \Pr\{\text{choosing } H_1 | H_1 \text{ is true}\} \\ & + c_{01} \pi_1 \Pr\{\text{choosing } H_0 | H_1 \text{ is true}\} \end{aligned}$$

It will further be assumed that the conditional densities of the observation  $x$  under both hypotheses are known. Letting  $p_0(x)$  and  $p_1(x)$  represent the conditional densities of  $x$  under the null and true hypotheses, respectively, the risk is

$$\begin{aligned} R = & c_{00} \pi_0 \int_{R_0} p_0(x) dx + c_{10} \pi_0 \int_{R_1} p_0(x) dx \\ & + c_{11} \pi_1 \int_{R_1} p_1(x) dx + c_{01} \pi_1 \int_{R_0} p_1(x) dx \quad . \end{aligned}$$

With some manipulation it can be shown<sup>13</sup> that choosing the decision boundary in this manner results in  $R_1$  including those values of  $x$  for which

$$\frac{p_1(x)}{p_0(x)} > \frac{\pi_0(c_{10} - c_{00})}{\pi_1(c_{01} - c_{11})} \quad .$$

The quantity on the left is called the likelihood ratio and is designated by  $\Lambda(x)$ . The quantity on the right represents a threshold and is labeled  $\Lambda_T$ . This test is called a likelihood ratio test and can be simply written

$$\Lambda(x) \stackrel{H_1}{\geq} \Lambda_T \quad .$$

$$\stackrel{H_0}{<}$$

The implementation of this test is shown in Fig. 2.2.

#### B. The Neyman-Pearson Lemma

In many cases neither the a priori probabilities  $\Pi_1$  and  $\Pi_0$  nor the costs of  $C_{ij}$  are known. In this study including these costs and probabilities would only complicate the evaluation of the optimal data processor. Therefore, a more general criterion is needed for the formulation of the detector considered here. The criterion is provided by Neyman and Pearson and is based on a theorem discussed below.

Before proceeding with the so-called Neyman-Pearson lemma, a few statistical terms related to hypothesis testing are introduced. The first of these terms is an error of the first kind. This refers to the third outcome of the decision process mentioned above (saying  $H_1$  when  $H_0$  is true). The conditional probability associated with this error is called the false alarm probability or the size or level of the test and is conventionally designated by  $\alpha$ . The conditional probability of a true alarm (saying  $H_1$  when  $H_1$  is true) is called the probability of detection, or the power of the test, and is generally designated by  $\beta$ . The Neyman-Pearson criterion consists of maximizing the power of the test  $\beta$  with the size of the test  $\alpha$  constrained to be less than or equal to some prescribed value.

The following presentation of the Neyman-Pearson lemma is taken from  
14  
Lehmann.

Let  $\phi(x)$  be the probability of announcing  $H_1$  when the observation is  $x$ . In the context of the Bayes test,  $\phi(x)$  would be either zero or one, depending on what region  $x$  lies within. Let  $E_0\{\phi(x)\}$  be the expected value of  $\phi(x)$  under the null hypothesis. In addition, let  $P_0$  and  $P_1$  be

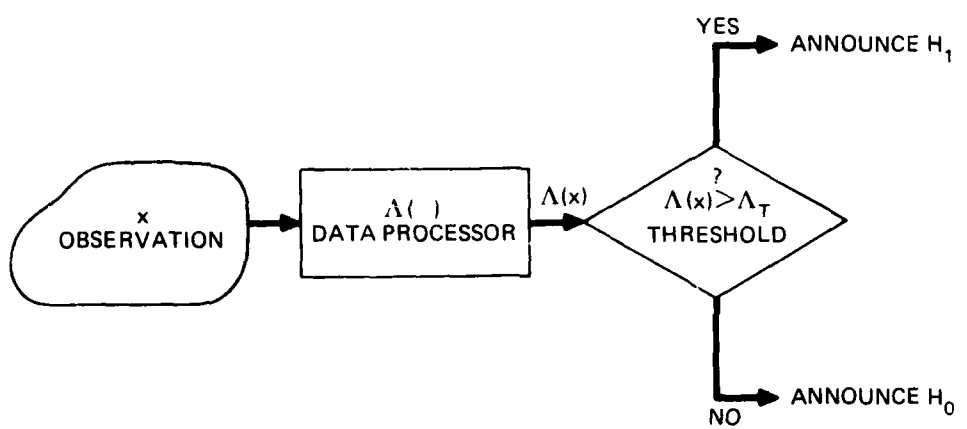


FIGURE 2.2  
LIKELIHOOD RATIO PROCESSOR

ARL:UT  
AS-81-272  
MEF - GA  
3-11-81

the probability distributions possessing derivatives  $p_o$  and  $p_1$ , respectively, with a measure  $\mu$ .

(i) Existence. For testing  $H_0:p_o$  against the alternative  $H_1:p_1$ , there exists a test  $\phi$  and a constant  $\Lambda_T$  such that

$$E_o\{\phi(x)\} = \alpha \quad (2.1)$$

and

$$\phi(x) = \begin{cases} 1 & \text{when } p_1(x) > \Lambda_T p_o(x) \\ 0 & \text{when } p_1(x) < \Lambda_T p_o(x) \end{cases} \quad (2.2)$$

(ii) Sufficient conditions for a most powerful test. If a test satisfies Eq. (2.1) and Eq. (2.2) for some  $\Lambda_T$ , then it is most powerful (maximum  $\beta$ ) for testing  $p_o$  against  $p_1$  at level  $\alpha$ .

(iii) Necessary condition for a most powerful test. If  $\phi$  is most powerful at level  $\alpha$  for testing  $p_o$  against  $p_1$ , then for some  $\Lambda_T$  it satisfies Eq. (2.2) almost everywhere with respect to the measure  $\mu$ . It also satisfies Eq. (2.1) unless there exists a test of size less than  $\alpha$  and with power equal to one.

The test  $\phi(x)$  in part (i) means that, given the observation  $x$ , hypothesis  $H_1$  is announced with probability one if  $(p_1(x)/p_o(x))$  is greater than  $\Lambda_T$ . Therefore,  $\phi(x)$  is a likelihood ratio test with threshold  $\Lambda_T$ . The threshold here is not a function of costs or a priori probabilities as in the Bayes test, but rather it is a function of the conditional densities  $p_o$  and  $p_1$  and the size of the test  $\alpha$ . To see this, consider Eq. (2.1) where

$$E_o\{\phi(x)\} = \int_{\text{All } x} \phi(x)p_o(x)dx = \int_{\left\{x: \frac{p_1(x)}{p_o(x)} > \Lambda_T\right\}} p_o(x)dx = \alpha \quad . \quad (2.3)$$

$\Lambda_T$  is chosen so that the value of the integral just equals  $\alpha$ . Note that, for  $\Lambda_T=0$ , the integral is over all  $x$  and is equal to unity. The power of the test at level  $\alpha$  is given by the expected value of  $\phi(x)$  under the hypothesis  $H_1$  as follows,

$$\beta = E_1\{\phi(x)\} = \int_{\text{All } x} \phi(x)p_1(x)dx = \int_{\left\{x: \frac{p_1(x)}{p_0(x)} > \Lambda_T\right\}} p_1(x)dx \quad (2.4)$$

Summarizing the test, it can be said that, given a false alarm probability  $\alpha$ , a threshold for the likelihood ratio  $\Lambda_T$  is chosen by Eq. (2.3). Given this  $\Lambda_T$  the detection probability  $\beta$  is computed from Eq. (2.4).

An evaluation of a given processor (i.e., given  $p_0$  and  $p_1$ ) can then be made by considering a plot of  $\beta$  versus  $\alpha$ . This plot is the so-called receiver operating characteristic (ROC) curve and is utilized herein to present the detector's performance. The thrust of the Neyman-Pearson lemma is that, given  $p_0$  and  $p_1$ , there exists no test whose ROC curve is above the curve associated with  $\phi(x)$ , the likelihood ratio test. If there were such a test it would be more powerful at the level  $\alpha$  where the curve was greater and hence would be a contradiction of the lemma.

### C. The Likelihood Ratio Detector

This section gives the assumptions upon which the detector is based. The specific detector structure is formulated and the method for performance evaluation is given.

#### 1. Assumptions

The major assumptions leading to the detector being studied here are as follows:

(1) Detection is a binary operation, i.e., one of two hypotheses must be chosen given an observation:  $H_0$ : observation due to noise alone, and  $H_1$ : observation due to signal-plus-noise. Only one observation is made even though in many practical sonar problems multiple "looks" at a potential target are possible before the detection decision is reached.

(2) Processing is done on a finite number of samples taken during a fixed time interval. This interval corresponds to the length of the known signal which is approximately equal to the pulse length of the transmission. In the sonar detection problem, the optimal detector would be time varying since the surface reverberation process is considered to be nonstationary.<sup>8</sup> In other words an actual system would process several fixed time intervals each corresponding to a different point in range.

(3) The signal is known, consisting of samples taken from an echo from a submerged styrofoam ball. Therefore, range and bearing to the target (when present) are known as well as the shape of the echo. The more general problem of a random signal with unknown target location is beyond the scope of this paper. As Middleton and Groginsky<sup>3</sup> point out, the assumption of known location is not purely academic. A series of such optimal detections might be carried out under this constraint at different ranges and bearings.

(4) Both system and ambient noise are considered to be negligible in relation to the noise level generated by surface reverberation. This is generally the case in most active sonar problems at close ranges.

(5) The noise process is Gaussian but not necessarily zero mean or stationary. The work by Frazer<sup>7,8</sup> indicated that this assumption is valid on a first order basis, i.e., the first order distribution function is Gaussian. The assumption that the process is jointly normal both in time and space is not quite as well substantiated. However, if only information about the second order moments is available, one may reasonably assume the process is Gaussian. This statement is based on the fact that, given an autocorrelation function of a random process, there always exists

a Gaussian random process possessing the same autocorrelation function. Therefore, the actual and the assumed processes are indistinguishable from the standpoint of what is known.

(6) The covariance of the noise process is known. In general this is not easy to determine; however, it is possible that the covariance function might be predicted.<sup>4-9</sup> For the optimum detector considered here, the covariance function is assumed known precisely.

(7) Signal and noise are additive. Since the noise considered in this study results from reverberation of sound waves from a rough surface, it is reasonable that these sound waves would add to an echo from a target at approximately the same range from the receiver as the surface.

## 2. Detector Formulation

In the previous development of the likelihood ratio detector, the observation  $x$  could have been a vector as well as a scalar quantity. Such is the case for the input to the data processor considered here. The development of this processor proceeds as follows. Consider  $M$  sets of received data,

$$\underline{v}(t) = [v_1(t), v_2(t), \dots, v_M(t)]^T ,$$

where  $[ ]^T$  indicates transpose operation, and  $v_i(t)$  is the waveform observed at the  $i$ th element over a fixed time interval. They are assumed to have been generated by either  $n_i(t)$  or  $s_i(t) + n_i(t)$  corresponding, respectively, to the hypothesis  $H_0$  that noise alone is present or to  $H_1$ , that signal-plus-noise is present. Next the  $v_i(t)$ 's are sampled in time, resulting in a set of  $M$  column vectors,

$$\underline{V} = [v_1, v_2, \dots, v_M]$$

where each  $v_i$  is the column vector,

$$\underline{v}_i = [v_i(t_1), v_i(t_2), \dots, v_i(t_N)]^T, \quad i = 1, M, \quad ,$$

and  $N$  is the number of samples taken during the fixed time interval. In the sampled data problem the two hypotheses are then

$$H_0 : \underline{V} = \underline{N}$$

and

$$H_1 : \underline{V} = \underline{S} + \underline{N} \quad ,$$

where

$$\underline{N} = [\underline{n}_1, \underline{n}_2, \dots, \underline{n}_M],$$

$$\underline{n}_i = [n_i(t_1), n_i(t_2), \dots, n_i(t_N)]^T, \quad i = 1, M, \quad ,$$

$$\underline{S} = [\underline{s}_1, \underline{s}_2, \dots, \underline{s}_M],$$

and

$$\underline{s}_i = [s_i(t_1), s_i(t_2), \dots, s_i(t_N)]^T, \quad i = 1, M \quad .$$

First the likelihood ratio is formed by

$$\Lambda(\underline{V}) = \frac{p_1(\underline{V})}{p_0(\underline{V})} \quad , \quad (2.5)$$

where  $p_1(\underline{V})$  and  $p_0(\underline{V})$  are the joint density functions of  $\underline{V}$  under  $H_1$  and  $H_0$ , respectively. Under  $H_0$ ,  $\underline{V} = \underline{N}$  and  $\underline{N}$  is assumed Gaussian; therefore,

$$p_0(\underline{V}) = c_{NM} \exp \left\{ -1/2 (\underline{V} - \underline{N})^T \underline{K}^{-1} (\underline{V} - \underline{N}) \right\} \quad ,$$

where

$$\begin{aligned}\underline{M} &= \text{noise mean vector} \\ &= E\{\underline{N}\},\end{aligned}$$

$$\begin{aligned}\underline{K} &= NM \times NM \text{ positive-definite, symmetric covariance matrix} \\ &= E\{(\underline{N}-\underline{M})(\underline{N}-\underline{M})^T\}, \text{ and}\end{aligned}$$

$$c_{NM} = (2\pi)^{-NM/2} \sqrt{|\underline{K}^{-1}|} .$$

Under  $H_1$ ,  $\underline{V} = \underline{S} + \underline{N}$  and the mean vector and covariance matrix are

$$E\{\underline{V}\} = E\{\underline{S} + \underline{N}\} = \underline{S} + \underline{M}$$

and

$$\begin{aligned}E\{(\underline{V}-E\{\underline{V}\})(\underline{V}-E\{\underline{V}\})^T\} &= E\{[\underline{S} + \underline{N} - (\underline{S} + \underline{M})][\underline{S} + \underline{N} - (\underline{S} + \underline{M})]^T\} \\ &= E\{(\underline{N}-\underline{M})(\underline{N}-\underline{M})^T\} \\ &= \underline{K} .\end{aligned}$$

Therefore,

$$p_1(\underline{V}) = c_{NM} \exp\{-1/2(\underline{V}-\underline{M}-\underline{S})^T \underline{K}^{-1} (\underline{V}-\underline{M}-\underline{S})\} .$$

Inserting these expressions for  $p_0$  and  $p_1$  into Eq. (2.5), simplifying, and taking the logarithm yields

$$\ln \Lambda(\underline{V}) = \underline{V}^T \underline{K}^{-1} \underline{S} - \underline{M}^T \underline{K}^{-1} \underline{S} - 1/2(\underline{S}^T \underline{K}^{-1} \underline{S}) .$$

The likelihood ratio test is

$$\ln \Lambda(\underline{V}) \stackrel{H_1}{\underset{H_0}{<}} \ln \Lambda_T$$

or, equivalently,

$$\lambda \triangleq \underline{V}^T \underline{K}^{-1} \underline{S} \stackrel{\substack{H_1 \\ \geq \\ H_0}}{>} \ln \Lambda_T + \underline{M}^T \underline{K}^{-1} \underline{S} + 1/2(\underline{S}^T \underline{K}^{-1} \underline{S}) \triangleq \lambda_T .$$

This last step is possible because the term on the left is the only one which depends on the observation  $\underline{V}$ . The other terms are functions of known quantities and consequently can be considered as part of the threshold which will be determined later.

Before proceeding further with the analysis, a few words are in order concerning the nature of the above data processor. Letting

$$\underline{B} = \underline{K}^{-1} \underline{S} , \quad (2.6)$$

the output  $\lambda$  can be written as the scalar product of  $\underline{V}$  and  $\underline{B}$ ,

$$\lambda = \underline{V}^T \underline{B} . \quad (2.7)$$

Also let

$$\underline{B} \triangleq [b_1, b_2, \dots, b_M]^T ,$$

where the  $b_i$ 's represent the filter coefficients for channel  $i$ . A block diagram of the multichannel likelihood ratio detector is shown in Fig. 2.3.

Consider  $\underline{K}^{-1}$  as a matrix of submatrices  $\underline{C}_{ij}$  each of order  $N$  (the number of time samples) as follows:

$$\underline{K}^{-1} = \begin{bmatrix} \underline{C}_{11} & \underline{C}_{12} & \dots & \underline{C}_{1M} \\ \underline{C}_{21} & \underline{C}_{22} & \dots & \underline{C}_{2M} \\ \vdots & \vdots & \ddots & \vdots \\ \underline{C}_{M1} & \underline{C}_{M2} & \dots & \underline{C}_{MM} \end{bmatrix} .$$

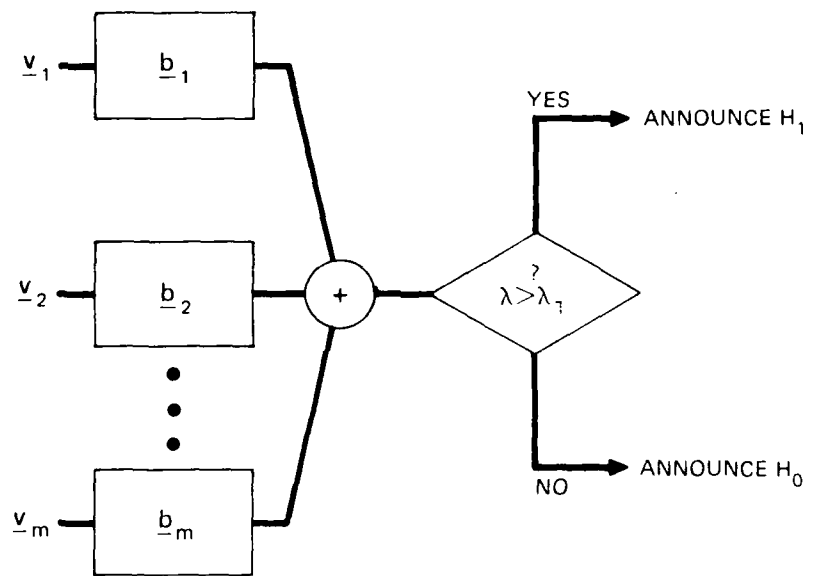


FIGURE 2.3  
MULTICHANNEL LIKELIHOOD RATIO PROCESSOR

ARL UT  
AS-81-273  
MEF - GA  
3-11-81

This notation is not meant to imply that  $C_{ij}$  is only a function of the covariance matrix between channels  $i$  and  $j$ . On the contrary, since  $C_{ij}$  represents a subsection of the inverse of the complete covariance matrix  $K$ , each of the elements of  $C_{ij}$  is a function of all the elements of  $K$ . Using this notation the elements  $b_i$  can be expressed as

$$b_i = \sum_{k=1}^M C_{ik} s_k, \quad i = 1, M .$$

It is interesting to note that in general the  $b_i$ 's depend not only on the signal and noise at channel  $i$ , but also on the signals and noise on each of the other channels as well.

Further insight into the detector structure may be gained by considering a few special cases. First consider a stationary Gaussian process with unit variance which is independent both in time and space. The inverse covariance matrix in that case is the identity matrix and the detector is a set of filters  $b_i$ ,  $i=1, M$ , each matched to the expected signal at channel  $i$ . The detector output  $\lambda$  in that case is

$$\lambda = \underline{v}^T \underline{b} = \sum_{i=1}^M \underline{s}_i^T \underline{v}_i$$

$$\lambda = \sum_{i=1}^M \sum_{j=1}^N s_i(t_j) v_i(t_j) .$$

The role of the covariance matrix may be observed by relaxing the assumption of stationarity. Thus, if the noise variance changes with time and channel, then the diagonal elements of the inverse covariance matrix are given by  $1/\sigma_{ij}^2$ , where  $\sigma_{ij}^2$  is the variance of the  $j$ th time sample on channel  $i$ . Consequently the vector of filter coefficients for channel  $i$  is

$$\underline{b}_i = \left[ \frac{s_i(t_1)}{\sigma_{i1}^2}, \frac{s_i(t_2)}{\sigma_{i2}^2}, \dots, \frac{s_i(t_N)}{\sigma_{iN}^2} \right]^T$$

It is apparent that the test statistic consists of weighting the input samples  $v_i(t_j)$  by  $s_i(t_j)/\sigma_{ij}^2$  as follows

$$\lambda = \sum_{i=1}^M \sum_{j=1}^N v_i(t_j) \frac{s_i(t_j)}{\sigma_{ij}^2}$$

In other words, if the signal is present and a particular sample is expected to be large in absolute value compared to the noise variance, then the sample  $v_i(t_j)$  is weighted accordingly.

Another interesting case arises when, in addition to the previous assumptions of stationarity, independence, and normality, it is also assumed that the signal is identical on each channel. (This condition could be created by adding a suitable time delay and weight factor in each channel, assuming the signal shape is identical on all channels.) Then the test statistic becomes

$$\lambda = \sum_{i=1}^M \underline{s}_i^T \underline{v}_i = \underline{s}_i^T \sum_{i=1}^M \underline{v}_i$$

and the processor amounts to a summation of the inputs at each channel followed by a single matched filter. This form of signal processing is prevalent in modern sonars.

### 3. Threshold Determination and Performance Prediction

In accordance with the Neyman-Pearson criterion, the threshold for the likelihood ratio test is chosen to achieve a given false alarm probability,  $\alpha$ . In general an analytic expression for the threshold as a function of  $\alpha$  is unobtainable and the relation must be determined

experimentally. Since the noise is assumed Gaussian in this study, the functional relationship can easily be derived.

If  $\lambda = \underline{V}^T \underline{K}^{-1} \underline{S}$ , then it represents a linear combination of the elements of  $\underline{V}$ , assumed Gaussian; therefore,  $\lambda$  is itself a normal random variable. Its expected value can be written

$$E\{\lambda\} = E\{\underline{V}^T \underline{K}^{-1} \underline{S}\} = E\{\underline{V}^T\} \underline{K}^{-1} \underline{S} \quad .$$

The variance of  $\lambda$  is

$$\begin{aligned} \text{Var}\{\lambda\} &\stackrel{\Delta}{=} \sigma_{\lambda}^2 = E\{[\lambda - E\{\lambda\}]^2\} \\ &= E\{[(\underline{V} - E\{\underline{V}\})^T \underline{K}^{-1} \underline{S}]^2\} \\ &= E\{\underline{S}^T (\underline{K}^{-1})^T (\underline{V} - E\{\underline{V}\}) (\underline{V} - E\{\underline{V}\})^T \underline{K}^{-1} \underline{S}\} \\ &= \underline{S}^T (\underline{K}^{-1})^T E\{(\underline{V} - E\{\underline{V}\}) (\underline{V} - E\{\underline{V}\})^T \underline{K}^{-1} \underline{S}\} \\ &= \underline{S}^T (\underline{K}^{-1})^T \underline{K} \underline{K}^{-1} \underline{S} \quad . \end{aligned}$$

Since  $\underline{K}$  is symmetric,  $(\underline{K}^{-1})^T = \underline{K}^{-1}$  and

$$\sigma_{\lambda}^2 = \underline{S}^T \underline{K}^{-1} \underline{S} \quad . \quad (2.8)$$

The threshold and the resulting power of the test are determined by considering the distribution of  $\lambda$  under the null and true hypotheses. Under hypothesis  $H_0$ ,  $\lambda$ 's mean value is

$$E_{\text{O}}\{\lambda\} \stackrel{\Delta}{=} m_{\text{O}} = E_{\text{O}}\{\underline{V}^T\} \underline{K}^{-1} \underline{S} \quad ,$$

or

$$m_{\text{O}} = \underline{M}^T \underline{K}^{-1} \underline{S} \quad .$$

Under hypothesis  $H_1$ , the mean of  $\lambda$  is

$$\begin{aligned} E_1\{\lambda\} &\stackrel{\Delta}{=} \underline{m}_1 = E_1\{\underline{V}^T\} \underline{K}^{-1} \underline{S} \\ &= (\underline{M}^T + \underline{S}^T) \underline{K}^{-1} \underline{S} \quad , \end{aligned}$$

or

$$\underline{m}_1 = \underline{M}^T \underline{K}^{-1} \underline{S} + \underline{S}^T \underline{K}^{-1} \underline{S} = \underline{m}_0 + \sigma_\lambda^2 \quad . \quad (2.9)$$

As was demonstrated earlier, the variance of  $\lambda$  is the same under both hypotheses and is represented by  $\sigma_\lambda^2$ . Thus it is apparent that the data processor reduces the samples of the vector random process  $\underline{V}$  to a sample of a normal random variable  $\lambda$ . Typical conditional probability density functions for  $\lambda$  given  $H_0$  and  $H_1$  are shown in Fig. 2.4 as  $p_{\lambda/H_0}(\lambda)$  and  $p_{\lambda/H_1}(\lambda)$ , respectively.

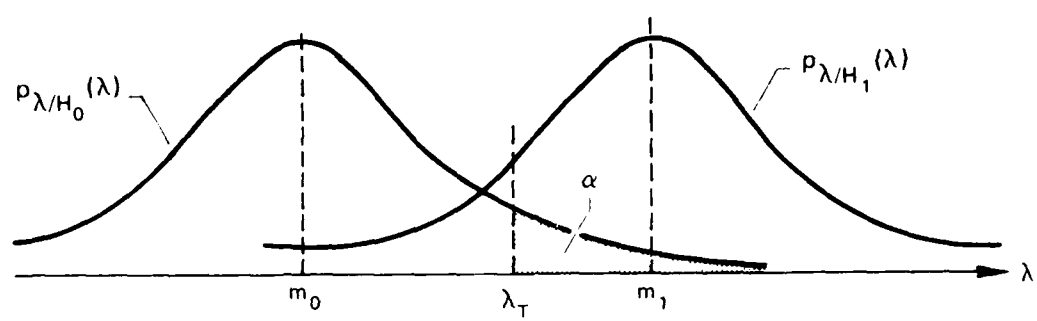
Since the likelihood ratio test can be represented by

$$\lambda \begin{array}{c} \stackrel{H_1}{>} \\ \stackrel{H_0}{<} \end{array} \lambda_T \quad ,$$

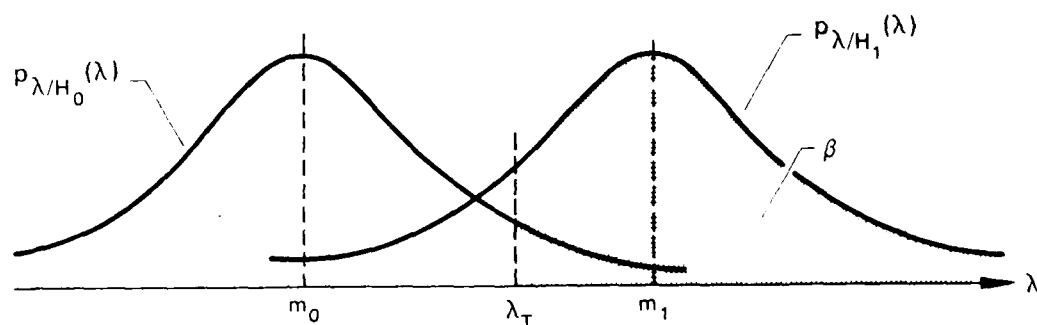
the false alarm probability is given by

$$\alpha = \int_{\lambda_T}^{\infty} p_{\lambda/H_0}(\lambda) d\lambda = \int_{\lambda_T}^{\infty} \frac{1}{\sigma_\lambda \sqrt{2\pi}} \exp \left[ -\frac{1}{2} \left( \frac{\lambda - \underline{m}_0}{\sigma_\lambda} \right)^2 \right] d\lambda \quad .$$

This probability is indicated by the shaded area in Fig. 2.4(a). Making the change of variables,



(a)  $\alpha$  = FALSE ALARM PROBABILITY



(b)  $\beta$  = DETECTION PROBABILITY

FIGURE 2.4  
TYPICAL CONDITIONAL PROBABILITY DENSITIES FOR THE TEST  
STATISTIC  $\lambda$  AND ASSOCIATED ERROR PROBABILITIES

ARL UT  
AS-81-274  
MEF - GA  
3-11-81

$$u = \frac{\lambda - m_o}{\sigma_\lambda}$$

yields

$$\alpha = \frac{1}{\sqrt{2\pi}} \int_{\frac{\lambda - m_o}{\sigma_\lambda}}^{\infty} e^{-u^2/2} du$$

or

$$1 - \alpha = \frac{1}{\sqrt{2\pi}} \int_{-\infty}^{\frac{\lambda - m_o}{\sigma_\lambda}} e^{-u^2/2} du$$

Defining

$$\phi(x) \triangleq \int_{-\infty}^x \frac{1}{\sqrt{2\pi}} e^{-u^2/2} du$$

generally referred to as the normal distribution function,<sup>15</sup> leads to an expression for  $\lambda_T$  as follows.

$$1 - \alpha = \phi \left\{ \frac{\lambda_T - m_o}{\sigma_\lambda} \right\}$$

$$\frac{\lambda_T - m_o}{\sigma_\lambda} = \phi^{-1}(1-\alpha) \quad , \quad (2.10)$$

and finally,

$$\lambda^T = m_0 + \sigma_\lambda \Phi^{-1}(1-\alpha) \quad . \quad (2.10)$$

Note that if the noise process is zero mean, then  $M=0$  and consequently  $m_0=0$ .

Given the threshold  $\lambda_T$ , the resulting detection probability  $\beta$  can be predicted by considering the density function for  $\lambda$  under the true hypothesis. Thus the expression for  $\beta$  is

$$\beta = \int_{\lambda_T}^{\infty} p_{\lambda/H_1}(\lambda) d\lambda = \int_{\lambda_T}^{\infty} \frac{1}{\sigma_\lambda \sqrt{2\pi}} \exp\left[-\frac{1}{2}\left(\frac{\lambda - m_1}{\sigma_\lambda}\right)^2\right] d\lambda \quad .$$

This probability is indicated by the shaded area in Fig. 2.4(b). By the appropriate change of variables,

$$\begin{aligned} \beta &= \int_{\frac{\lambda_T - m_1}{\sigma_\lambda}}^{\infty} \frac{1}{\sqrt{2\pi}} e^{-u^2/2} du \\ &= 1 - \int_{-\infty}^{\frac{\lambda_T - m_1}{\sigma_\lambda}} \frac{1}{\sqrt{2\pi}} e^{-u^2/2} du \\ \beta &= 1 - \Phi\left(\frac{\lambda_T - m_1}{\sigma_\lambda}\right) \quad . \quad (2.11) \end{aligned}$$

An expression for  $\beta$  as a function of  $\alpha$  may be obtained by substituting Eqs. (2.9) and (2.10) in Eq. (2.11). Therefore,

$$\begin{aligned}\beta &= 1 - \Phi \left\{ \frac{[m_o + \sigma_\lambda \Phi^{-1}(1-\alpha)] - m_1}{\sigma_\lambda} \right\} \\ &= 1 - \Phi \left\{ \frac{m_o + \sigma_\lambda \Phi^{-1}(1-\alpha) - m_1 - \sigma_\lambda^2}{\sigma_\lambda} \right\},\end{aligned}$$

or

$$\beta = 1 - \Phi \left\{ \Phi^{-1}(1-\alpha) - \sigma_\lambda \right\} \quad . \quad (2.12)$$

This is the predicted ROC curve for the detector and is presented in Fig. 2.5 for several values of  $\sigma_\lambda$ . Horton<sup>1</sup> had demonstrated that  $\sigma_\lambda$  is related to the output signal-to-noise ratio. Intuitively this can be seen by observing that the separation between the two curves in Fig. 2.4 is  $\sigma_\lambda^2$ . Since the detector's performance improves with increasing  $\sigma_\lambda$ , one might be led to consider Eq. (2.12) in that regard. If the noise were independent of the signal then  $\underline{S}$  could be chosen to maximize  $\sigma_\lambda$ . However, in the active sonar problem the noise is very definitely related to  $\underline{S}$  since both are produced by the transmitted pulse. Thus, any change in  $\underline{S}$  caused by altering the transmission results in a different covariance matrix.

One of the objectives of this study is to compare the predicted ROC curves with experimental results obtained by processing experimentally acquired acoustic data with the proposed detector. The manner in which the experimental ROC curves are derived will be described in Section IV.

#### D. Sampling Technique

It was stated earlier that the input to the data processor would be a set of samples from a fixed time interval. Since the processor's computational complexity is roughly proportional to the square of the number of samples (due to the matrix inversion of  $\underline{K}$ ), the sampling frequency and

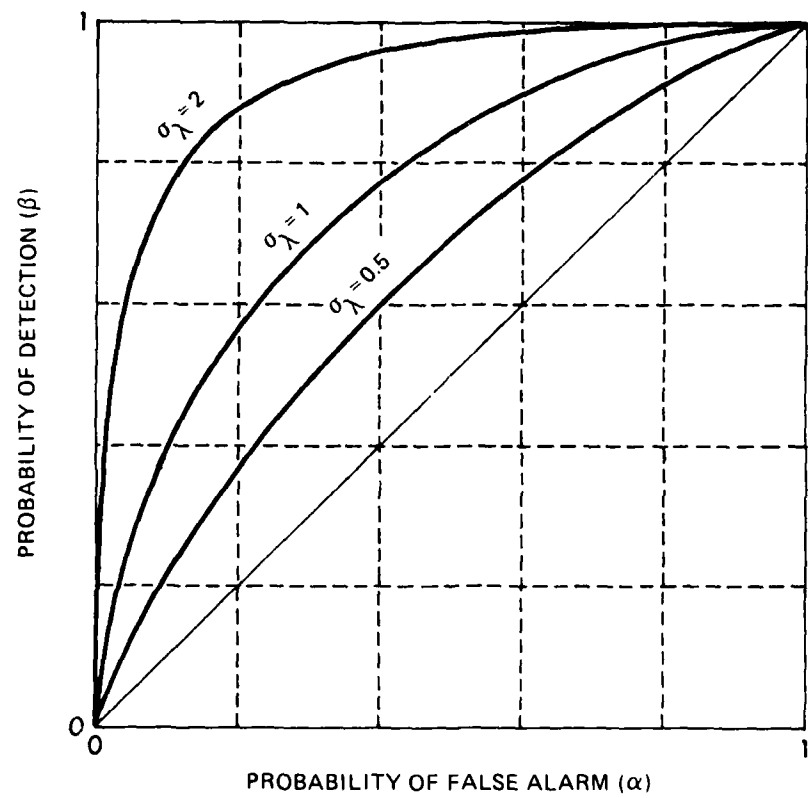


FIGURE 2.5  
PREDICTED DETECTOR PERFORMANCE  
WITH  $\sigma_\lambda$  AS A PARAMETER

ARL-UT  
AS-81-275  
MEF - GA  
3-11-81

techniques are major concerns. In this section the sampling method is described.

In many sonar applications the signals of interest are bandlimited to the extent that most of the energy is concentrated within a band of frequencies. This is generally the case with an active sonar which transmits acoustic energy at a bandwidth which is small compared to the carrier frequency. Also, the first stage of signal processing by the receiver usually involves bandpass filtering. Such is the case for the signals considered here for processing by the likelihood ratio detector.

To facilitate the discussion of the sampling technique, the signal is assumed to be a real function of time which is strictly bandlimited to the frequency interval  $(f_o - W/2) < |f| < (f_o + W/2)$ . Furthermore, it is assumed that the bandwidth  $W$  is small compared to the carrier frequency  $f_o$ . Such a signal can be represented in the time domain by

$$v(t) = A(t) \cos[2\pi f_o t + \phi(t)] , \quad (2.13)$$

where  $A(t)$  and  $\phi(t)$  are the amplitude and phase functions, respectively.

The quadrature representation obtained by the identity  $\cos(A+B) = \cos A \cos B - \sin A \sin B$  is

$$v(t) = X(t) \cos(2\pi f_o t) + Y(t) \sin(2\pi f_o t) ,$$

where

$$X(t) = A(t) \cos \phi(t) , \text{ and}$$

$$Y(t) = -A(t) \sin \phi(t) .$$

$X(t)$  and  $Y(t)$  are called, respectively, the in phase and out of phase quadrature components of  $v(t)$  and are bandlimited to the interval  $|f| < W/2$ .

$X(t)$  and  $Y(t)$  can be completely represented by their samples taken at a minimum rate of  $W$  samples per second, commonly referred to as the Nyquist rate.<sup>16</sup>

One method of obtaining samples of  $X(t)$  and  $Y(t)$  consists of heterodyning  $v(t)$  appropriately to produce the two quadrature components and then sampling. A preferred method is to obtain samples of  $X(t)$  and  $Y(t)$  by sampling  $v(t)$  directly in the manner presented by Pitt and Grace.<sup>17-19</sup> A simplified version of the technique is described here.

Samples of  $X(t)$  are obtained by sampling  $v(t)$  at the times  $t=nk/f_o$ ,  $n=1,2,3,\dots,N/2$ , where the sampling parameter  $k$  is a positive integer which determines the time interval between samples of  $X(t)$  in multiples of  $1/f_o$ , and  $N$  is the total number of samples from both components. To ensure that samples of  $X(t)$  are taken at a rate no less than the bandwidth  $W$ ,  $k$  must be less than or equal to the largest integer that is less than or equal to  $f_o/W$ . If  $v(t)$  is also sampled at the same frequency but at times  $t=(nk/f_o)+(1/4f_o)$ ,  $n=1,2,3,\dots,N/2$ , samples of  $Y(t)$  are produced. These relationships are obtained by substituting the above times in Eq. (2.13). For more details the reader is referred to Refs. 17-19.

Oftentimes the amplitude and phase functions of  $v(t)$  are of interest. They may be computed from samples of  $X(t)$  and  $Y(t)$  as follows:

$$A(t) = \sqrt{X^2(t) + Y^2(t)} ,$$

and

$$\phi(t) = \tan^{-1} \frac{-Y(t)}{X(t)} .$$

However, since the samples of  $Y(t)$  occur a quarter cycle of the carrier later ( $1/4f_o$ ) than those of  $X(t)$ , the following approximation must be made.

$$Y\left(\frac{nk}{f_o} + \frac{1}{4f_o}\right) \approx Y\left(\frac{nk}{f_o}\right)$$

If  $W$  is small compared to  $f_o$ , then  $Y(t)$  is slowly varying with respect to  $\cos(2\pi f_o t)$  and the approximation is a good one.

To study the effect of sampling frequency on the detector's performance the quadrature sampling technique is employed. An input vector  $\underline{v}_i$  from a given channel  $i$  consists of quadrature samples of  $v_i(t)$  as follows:

$$\underline{v}_i = [v_i(t_1), v_i(t'_1), v_i(t_2), v_i(t'_2), \dots, v_i(t_{N/2}), v_i(t'_{N/2})] \quad , \quad (2.14)$$

where

$$t_n = \frac{nk}{f_o} \quad , \quad (2.15)$$

corresponding to the in phase component, and

$$t'_n = \frac{nk}{f_o} + \frac{1}{4f_o} \quad , \quad (2.16)$$

yielding samples of the out of phase component. The effect of sampling frequency on detector performance is observed by varying the sampling parameter  $k$ .

### III. EXPERIMENTAL PROCEDURE

This chapter describes the acquisition of data used in the evaluation of the likelihood ratio detector. These data consist of measurements of reverberation from the lake surface and echoes from a styrofoam sphere. The reverberation data were obtained in an experiment conducted in September 1974. This experiment is described briefly here and in greater detail in Ref. 9. A second experiment was conducted in July 1975, in which the styrofoam sphere echoes were recorded using the same equipment as the 1974 experiment. A notable improvement relating to the alignment of data from different channels (see Section IV.A) was made in the second experiment. The second data collection exercise was also conducted to gather additional reverberation data; however, these data were deemed unsuitable for this study due to a low interchannel coherence. A description of the arrangement and location of equipment is given including types of sonar transmissions utilized. Finally, the analog recording and analog-to-digital conversion processes are discussed.

#### A. Data Acquisition Site and Environmental Conditions

The data used in this study were obtained at Applied Research Laboratories Lake Travis Test Station (LTTS).<sup>20</sup> Figure 3.1, adapted from Ref. 20, indicates the geographic location of LTTS. Since LTTS is on the south end of the lake, data are taken with the wind from a northerly direction. This produces a fairly rough surface so that meaningful reverberation phenomena may be observed. Table I presents the pertinent environmental factors observed during the reverberation and target echo experiments.

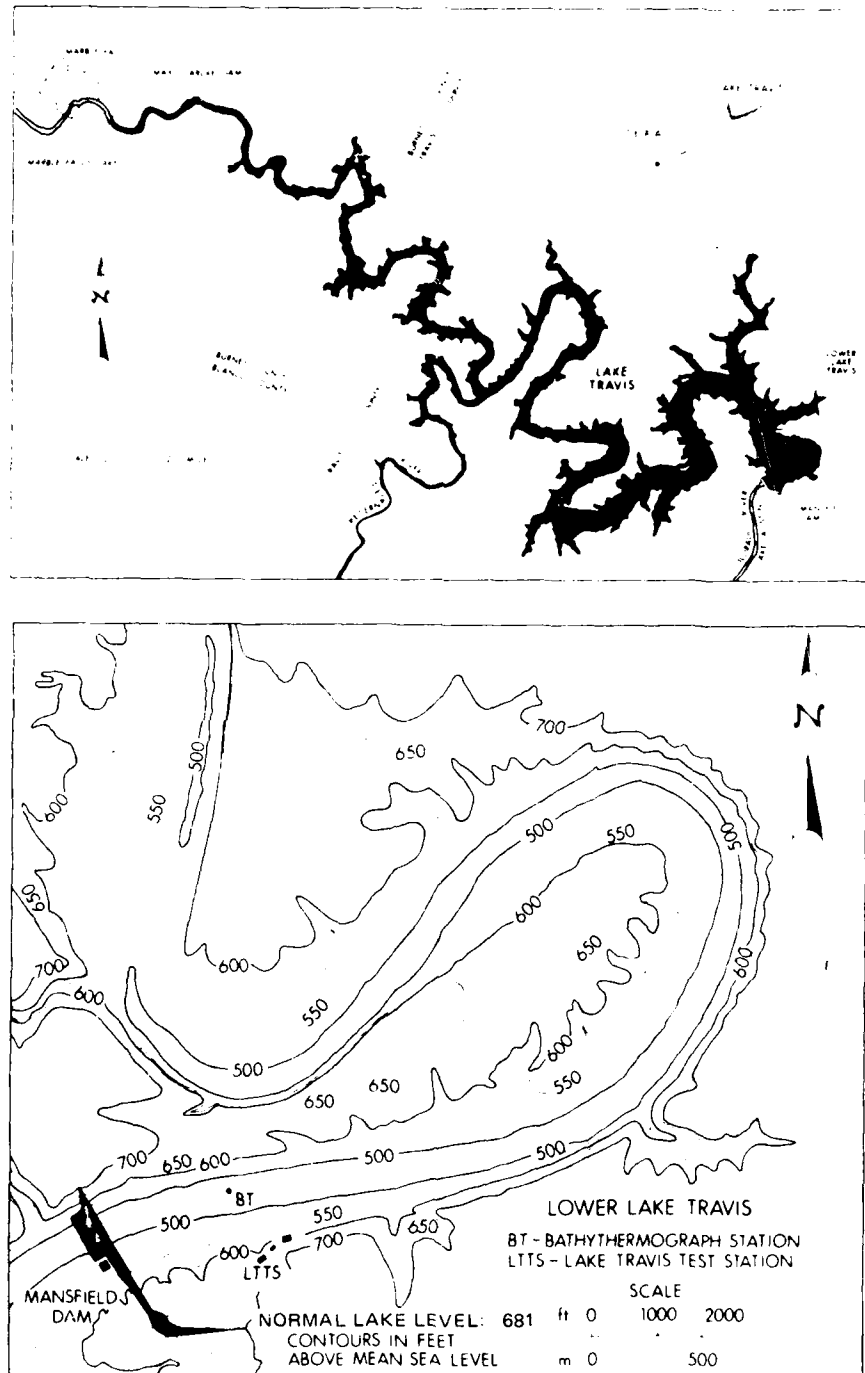


FIGURE 3.1  
LOCATION OF LAKE TRAVIS TEST STATION

ARL-UT  
AS-81-276  
MEF-GA  
3-11-81

TABLE I  
ENVIRONMENTAL FACTORS OF REVERBERATION AND  
TARGET ECHO EXPERIMENTS

Data Type	Reverberation, Pulsed Continuous Wave (cw) Signal	Reverberation, Pulsed Linear Frequency Modulated (LFM) Signal	Target Echo, cw and LFM Signals
Date	25 September 1974	25 September 1974	10 July 1975
Time	16:15	17:25	16:30
Temperature in water	24.7°C isothermal	24.7°C isothermal	Surface 31.1°C Bottom 25.6°C
Sound Velocity	1496 m/sec	1496 m/sec	1507 m/sec
Wind Direction	NW≈NNW	north	north
Wind Speed	7.6-8 m/sec	9.4 m/sec	2.7 m/sec
Wave Height	0.3 m	0.3 m	0.3 m
Direction of Hydrophone	north	north	NNW
Water Depth at Hydrophone	29 m	29 m	29 m

### B. Description of Transducer Array

The transducer array consisted of a linear receiving array with a projector rigidly attached (see Fig. 3.2, adapted from Ref. 9). The receiving array was constructed of 20 rectangular elements with planar surfaces. Each element was 10.2 cm high and 4.95 cm wide. The horizontal separation (edge to edge) between elements was 0.15 cm. Only the center six elements were used in these experiments. The projector was also planar and rectangular with a horizontal dimension of 6.6 cm and a vertical dimension of 38.1 cm.

Beam patterns (intensity versus angle) for receiver elements and projector are documented in Ref. 9. The beam patterns were not measured during the second experiment (July 1975); however, they are assumed to be comparable to the patterns measured in the 1974 experiment.

### C. Reverberation Measurement

The geometry for the reverberation experiment is shown in Fig. 3.3 (adapted from Ref. 9). A transducer array was placed at a depth of 3.6 m and tilted approximately 16° toward the surface. Two transmit signals were employed:

- (1) 1.0 msec pulsed 80 kHz continuous wave (cw) signal, and
- (2) 1.0 msec pulsed linear frequency modulated (LFM) signal with a 10 kHz sweep centered at 80 kHz.

A total of 99 reverberation returns were generated for the cw data and 103 for the LFM data. The time separation between consecutive transmissions was 0.6 sec.

### D. Target Echoes

The target utilized in this study consisted of several styrofoam disks held together by metal plates (see Fig. 3.4). The overall dimensions are approximately 30.5 cm diameter and 30.5 cm height. Echoes from this reflector were obtained by tilting the transducer array below the

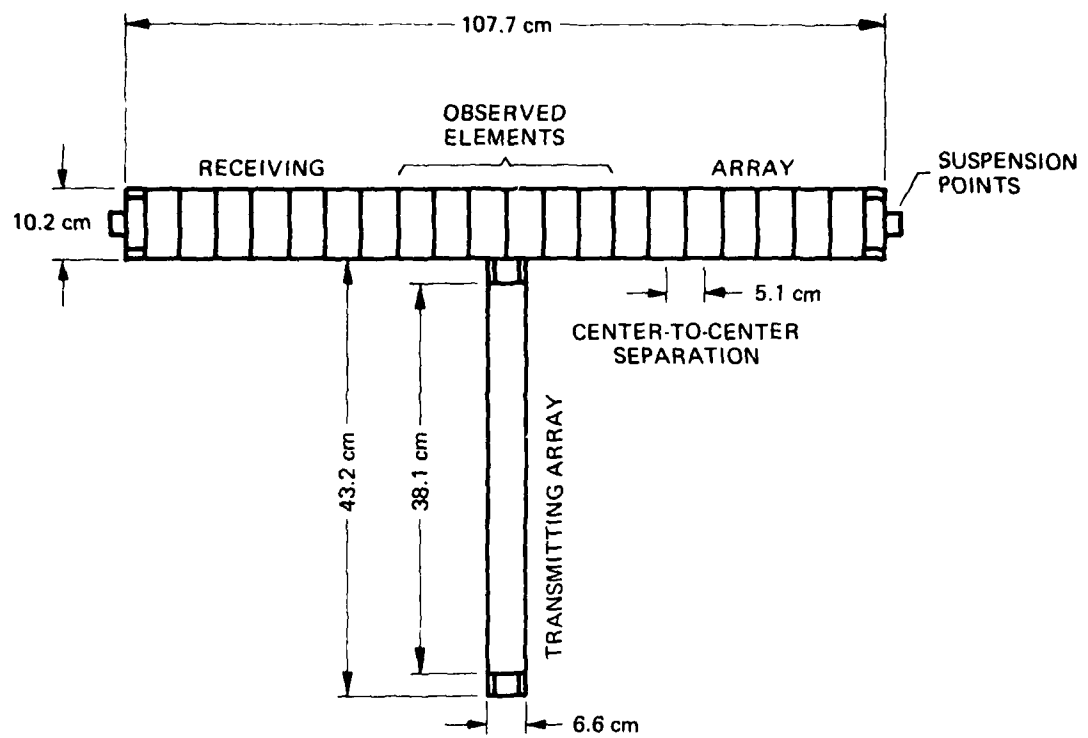


FIGURE 3.2  
A FRONT VIEW OF THE TRANSDUCER ARRAY

ARL:UT  
AS-81-277  
MEF - GA  
3-11-81

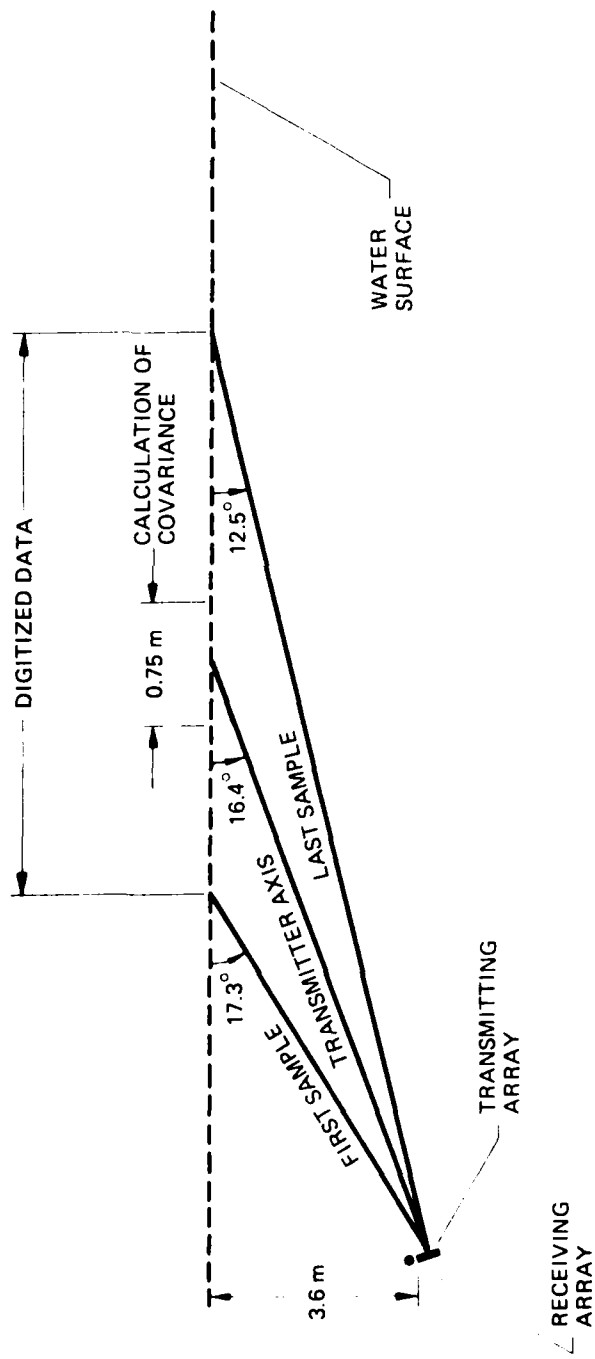


FIGURE 3.3  
A VERTICAL PROFILE OF THE GEOMETRIC FEATURES  
OF THE REVERBERATION EXPERIMENT

ARL:UT  
AS-81-278  
MEF - GA  
3-11-81

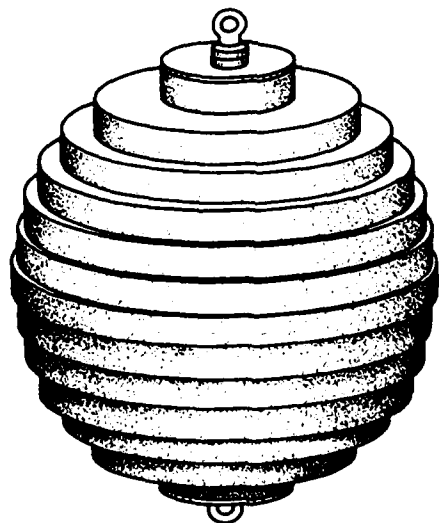
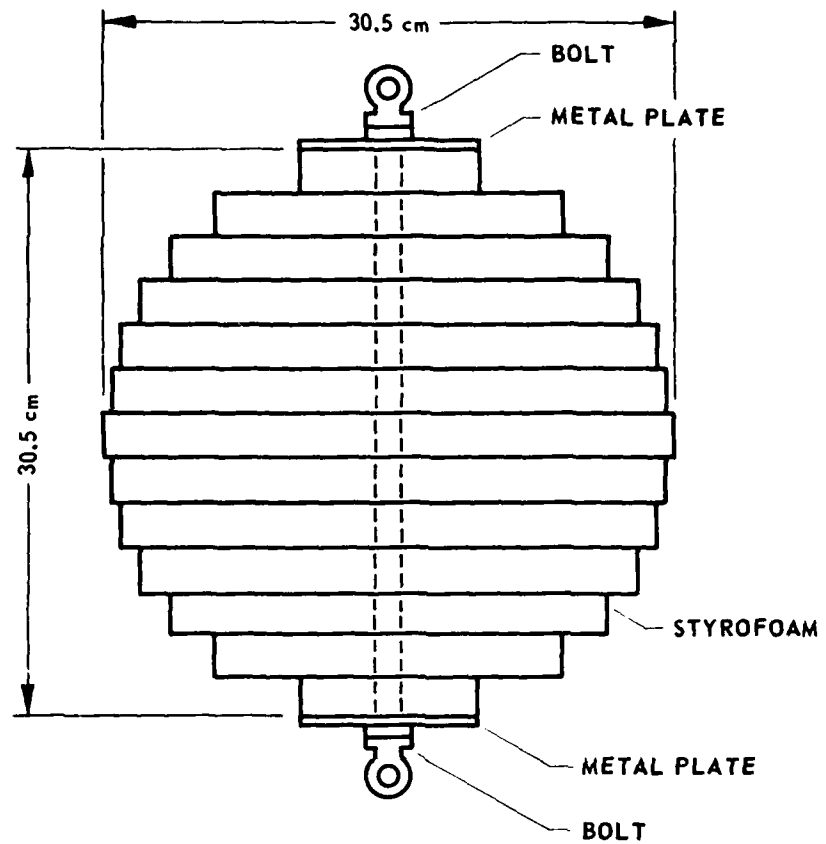


FIGURE 3.4  
UNDERWATER SOUND REFLECTOR

ARL:UT  
AS-80-582  
AJE.GA  
1-16-80

horizontal so that the projector axis pointed toward the target, which was located at a horizontal range of 60 m and submerged to a depth of 9 m. This depression angle was chosen to minimize the surface reverberation level so that high signal-to-background echoes might be obtained. The transmit signals employed here were the same as those used in the reverberation experiment.

#### E. Data Acquisition

In this section the data acquisition system employed in the July 1975 experiment is described. The earlier experiment was similar and is described in Ref. 9.

A block diagram of the recording system is shown in Fig. 3.5. As shown in the diagram, several signals are summed with the received signal before being led to the tape recorder. These signals are included to facilitate the analog-to-digital (A/D) conversion process. A block diagram of the A/D system is shown in Fig. 3.6, adapted from Ref. 9. A 12-bit A/D is used covering a range of  $\pm 10$  V.

A clock signal was added to each channel to serve as a sample clock for the A/D converter. Providing this signal on every channel permits later compensation for the effects of the tape recorder's dynamic skew on the relative phase relationships between channels. The A/D samples the data channel at every zero crossing of the 160 kHz clock signal, thus yielding a uniform sampling frequency of 320 kHz ( $4f_o$ ).

The sync signal was added to provide a start pulse for the A/D converter. As seen in Fig. 3.6, the A/D was started by triggering an oscilloscope which in turn provided an A/D start signal after an adjustable delay.

Since each tape recorder channel was played back and digitized separately, a method is required for ensuring that the time base is the same for all channels. This is accomplished by recording a Barker coded

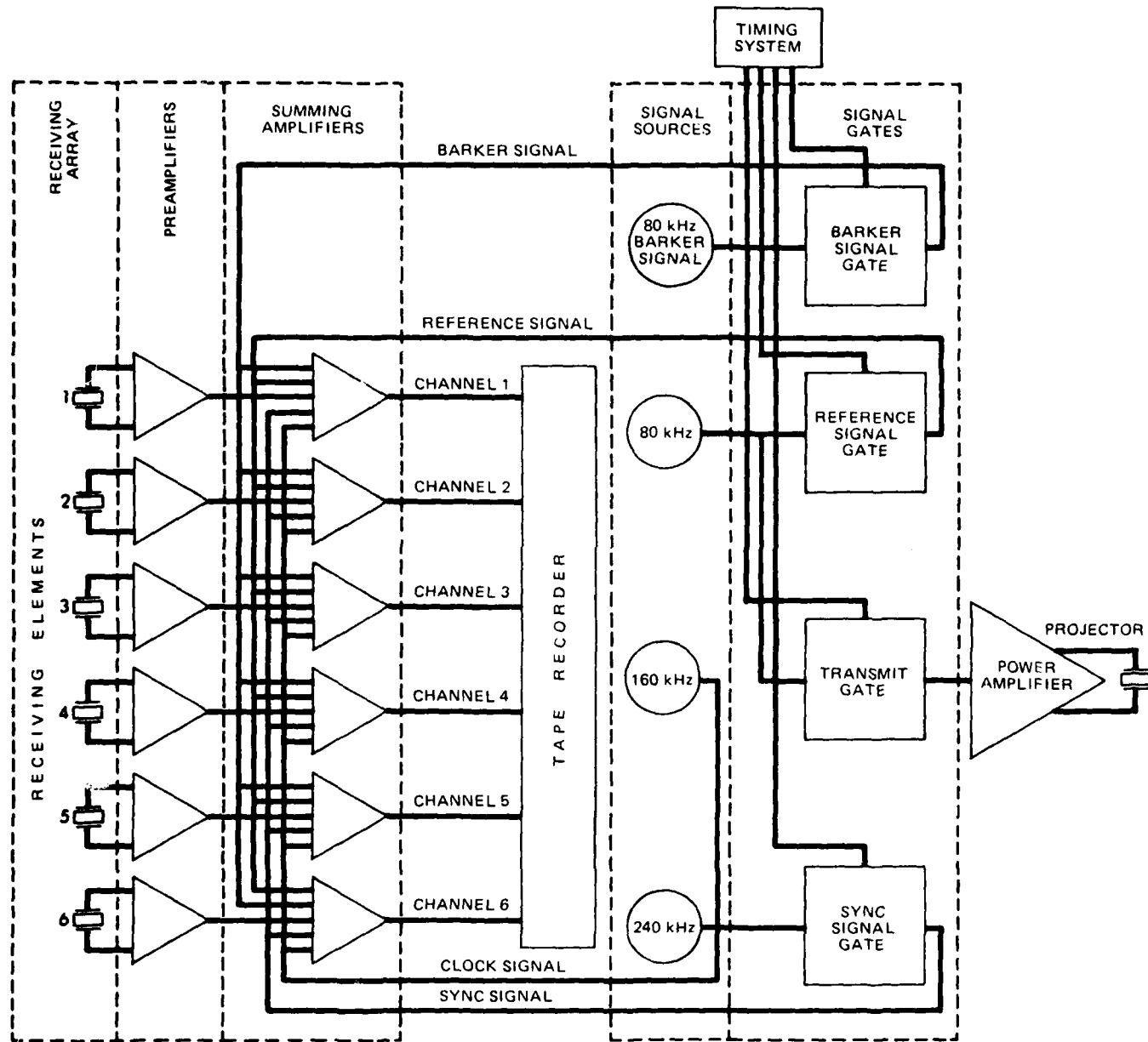


FIGURE 3.5  
A BLOCK DIAGRAM OF THE ANALOG DATA RECORDING SYSTEM

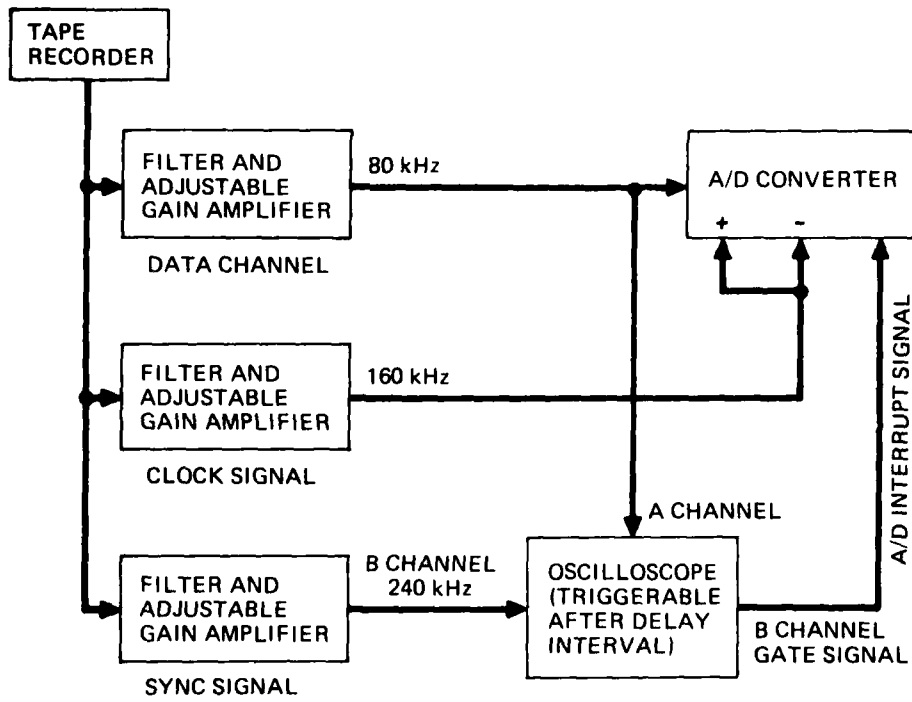


FIGURE 3.6  
BLOCK DIAGRAM OF DIGITIZATION EQUIPMENT

ARL:UT  
AS-81-280  
MEF-GA  
3-11-81

pulse<sup>21</sup> at 80 kHz center frequency shortly after the transmit signal. This pulse consisted of a 16-bit binary code with each "1" bit represented by two cycles of the 80 kHz carrier at one phase angle and each "0" bit by two cycles 180° out of phase with the "1" bits. The particular code employed was 0001010110011111. By correlating the Barker pulse on a reference channel and ping with that from every other channel and ping, the error in the time base is minimized (see Section IV.A).

Time base error is further reduced by also recording a reference cw pulse at 80 kHz immediately following the Barker pulse. If the time base is correct for all pings and channels, then the constant phase of the reference pulse will be the same in all cases. Using this reference pulse, data may be corrected for any difference found. While the above procedure is not foolproof, the results (described in Section IV.A) indicate the method is highly satisfactory.

The data collection procedure was very similar in the 1974 experiment except no Barker pulse was recorded.

#### IV. EXPERIMENTAL RESULTS

The results of the experimental performance analysis are presented in this section. First, the computational procedure for aligning the data in time is discussed. The computation of the covariance matrix estimate used by the detector is included as well as plots of the cw and LFM matrices. Details of the detector evaluation are presented including the computation of experimental ROC curves. The analysis of results considers the detector performance for various parameters of interest and concludes with a comparison of the optimum detector to several simplified processors.

##### A. Alignment of Digital Samples

The first area of experimental results to be discussed concerns the alignment of data from different pings and different channels of the recording system. The method consists of time shifting data from one event with respect to another by an amount which yields the greatest crosscorrelation of the two Barker pulses. In other words, when the Barker pulses "line up" the entire data sequence is assumed to be reasonably aligned in time. The Barker code was utilized so that the crosscorrelation function would have a more well defined peak compared to some other waveform such as a cw pulse. Even though much of the Barker code is distorted by the 10 kHz filters prior to digitization, the Barker pulse data did exhibit this sharp peak.

Since the filtered Barker pulses are essentially bandlimited functions, the crosscorrelation of two of them will also be narrowband and consequently will possess an envelope as a function of time shift.<sup>19</sup> To minimize the error in time shift required to produce the maximum correlation, the envelope is considered rather than values of the

crosscorrelation function itself. Thus the alignment procedure consists of computing a crosscorrelation envelope for several time differences between a given event and a reference event and shifting the data accordingly. A more detailed explanation of the computational procedure is given in the appendix. As a final check, the phases of the cw reference pulses for the two data sequences are compared after the data have been shifted. In all cases the resulting phase differences were less than  $25^\circ$ . The data were further corrected for this phase difference by rotating each pair of quadrature samples<sup>19</sup> as follows:

$$X'(na) = X(na) \cos\Delta\phi + Y(na) \sin\Delta\phi \quad ,$$

and

$$Y'(na) = Y(na) \cos\Delta\phi - X(na) \sin\Delta\phi \quad ,$$

where  $\Delta\phi$  is the phase difference between reference pulses. Once the selected data segment had been properly aligned, it was output to digital tape for further processing. The selected segment started at approximately 16.0 msec after transmission and extended for 6.25 msec.

In the reverberation data taken during the 1974 experiment, no Barker pulse was available so the crosscorrelation procedure was applied to the constant phase reference pulse. Although the results appear satisfactory, the use of a coded pulse should make the procedure more reliable.

B. Computation of the Covariance Matrix Estimate and Data Segment Selection

The covariance matrix involved in the optimum detector was defined previously by:

$$\underline{K} = E\{ (\underline{N}-\underline{M})(\underline{N}-\underline{M})^T \} \quad .$$

The elements of this matrix are estimated from an ensemble average over approximately 100 events. The estimated matrix is employed to detect a known signal added to these same 100 events. Each element of the estimated matrix represents the covariance between the  $m$ th time sample of the  $i$ th element and the  $n$ th time sample of the  $j$ th element and is computed by

$$\hat{K}_{ij}(t_m, t_n) = \frac{1}{\Gamma} \sum_{\gamma=1}^{\Gamma} n_i(t_m, \gamma) n_j(t_n, \gamma) - \left\{ \frac{1}{\Gamma} \sum_{\gamma=1}^{\Gamma} n_i(t_m, \gamma) \right\} \left\{ \frac{1}{\Gamma} \sum_{\gamma=1}^{\Gamma} n_j(t_n, \gamma) \right\} , \quad (4.1)$$

for  $i, j = 1$ , number of elements, and

$m, n = 1$ , number of samples

where  $n_i(t_m, \gamma)$  is the  $m$ th time sample from the  $i$ th element on the  $\gamma$ th event and  $\Gamma$  represents the number of events in the ensemble.

This matrix may be presented graphically by considering the quadrature representation as Frazer does in Ref. 8. This representation is

$$\begin{aligned} \hat{K}_{ij}(t_m, t_n) = & \hat{X}_{ij}(t_m, t_n) \cos \omega_0 [t_n - t_m] \\ & + \hat{Y}_{ij}(t_m, t_n) \sin \omega_0 [t_n - t_m] , \end{aligned}$$

where

$$\hat{X}_{ij}(t_m, t_n) = \frac{1}{2\Gamma} \sum_{\gamma=1}^{\Gamma} [x_i(t_m, \gamma) x_j(t_n, \gamma) + y_i(t_m, \gamma) y_j(t_n, \gamma)] ,$$

$$\hat{Y}_{ij}(t_m, t_n) = \frac{1}{2\Gamma} \sum_{\gamma=1}^{\Gamma} [x_i(t_m, \gamma) y_j(t_n, \gamma) - y_i(t_m, \gamma) x_j(t_n, \gamma)] ,$$

and

$$x_i(t_m, \gamma) = x_i'(t_m, \gamma) - \frac{1}{\Gamma} \sum_{\gamma=1}^{\Gamma} x_i'(t_m, \gamma)$$

$$y_i(t_m, \gamma) = y_i'(t_m, \gamma) - \frac{1}{\Gamma} \sum_{\gamma=1}^{\Gamma} y_i'(t_m, \gamma) \quad ,$$

with  $[x_i'(t_m, \gamma), y_i'(t_m, \gamma)]$  equal to, respectively, the in phase and quadrature components of  $n_i(t_m, \gamma)$

The envelope and phase of the elements of the covariance matrix are determined in the usual manner from the polar representation

$$\hat{K}_{ij}(t_m, t_n) = \hat{E}_{ij}(t_m, t_n) \cos\left\{\omega_o[t_n - t_m] + \hat{\phi}_{ij}(t_m, t_n)\right\} \quad .$$

Thus the envelope is computed by

$$\hat{E}_{ij}(t_m, t_n) = \left\{ \hat{x}_{ij}^2(t_m, t_n) + \hat{y}_{ij}^2(t_m, t_n) \right\}^{1/2} \quad , \quad (4.2)$$

and the phase

$$\hat{\phi}_{ij}(t_m, t_n) = \tan^{-1} \left\{ \frac{\hat{y}_{ij}(t_m, t_n)}{\hat{x}_{ij}(t_m, t_n)} \right\} \quad . \quad (4.3)$$

The elements of the normalized covariance matrix are given by<sup>8</sup>

$$\hat{k}_{ij}(t_m, t_n) = \frac{\hat{K}_{ij}(t_m, t_n)}{\left\{ \hat{K}_{ii}(t_m, t_m) \hat{K}_{jj}(t_n, t_n) \right\}^{1/2}} \quad ,$$

and the envelope of  $\hat{k}_{ij}(t_m, t_n)$  by

$$\hat{e}_{ij}(t_m, t_n) = \frac{\hat{E}_{ij}(t_m, t_n)}{\sqrt{\hat{K}_{ii}(t_m, t_m) \hat{K}_{jj}(t_n, t_n)}} . \quad (4.4)$$

Plots of normalized envelope and phase for the covariance matrices used in this study are shown in Figs. 4.1-4.4. While these figures represent only a slice (fixed  $t_m$ ) of the matrix used by the detector, the functions should have similar form for all values of  $t_m$ .

The particular time segment shown in the covariance plots was selected in the following manner. A segment 1 msec long was chosen which corresponds to the approximate length of the target echoes. Since one intent of this study is to evaluate the effect on the detection problem of considering the covariance between channels, it is desirable to choose the 1 msec segment in the reverberation data where a significant covariance occurs between channels. To determine this point the covariance function was computed for zero time shift versus time of observation, i.e.,

$$\hat{K}_{ij}(t_m, t_m) \text{ versus } t_m$$

for each pair of adjacent channels. The envelope (Eq. (4.2)), phase (Eq. (4.3)), and normalized envelope (Eq. (4.4)) for elements one and two ( $\hat{K}_{12}(t_m, t_m)$ ) are presented in Figs. 4.5 and 4.6 for the cw and LFM data, respectively. The covariance  $\hat{K}_{23}$  and  $\hat{K}_{34}$  were similar to  $\hat{K}_{12}$  while  $\hat{K}_{45}$  and  $\hat{K}_{56}$  indicated a much lower interchannel coherence. For this reason only elements 1-4 are considered in the sequel. The selected data segment is indicated by dashed lines and consists of 320 samples from  $t = 18.4$  msec to  $t = 19.4$  msec after transmission.

Since the effect of considering noise (reverberation) on separate channels is being evaluated here, it is desirable to have the same average level of noise power on each channel. If one channel had a lower

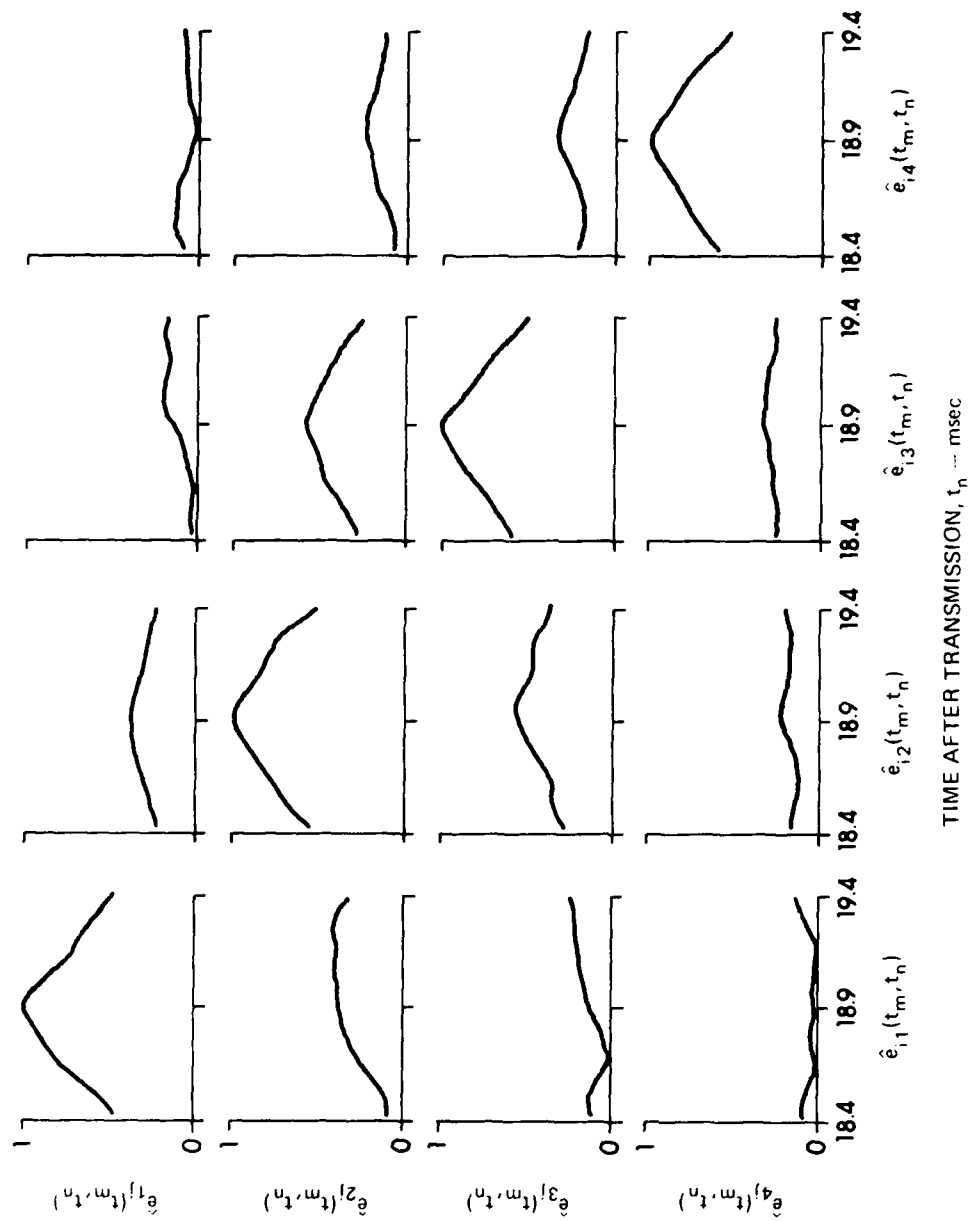
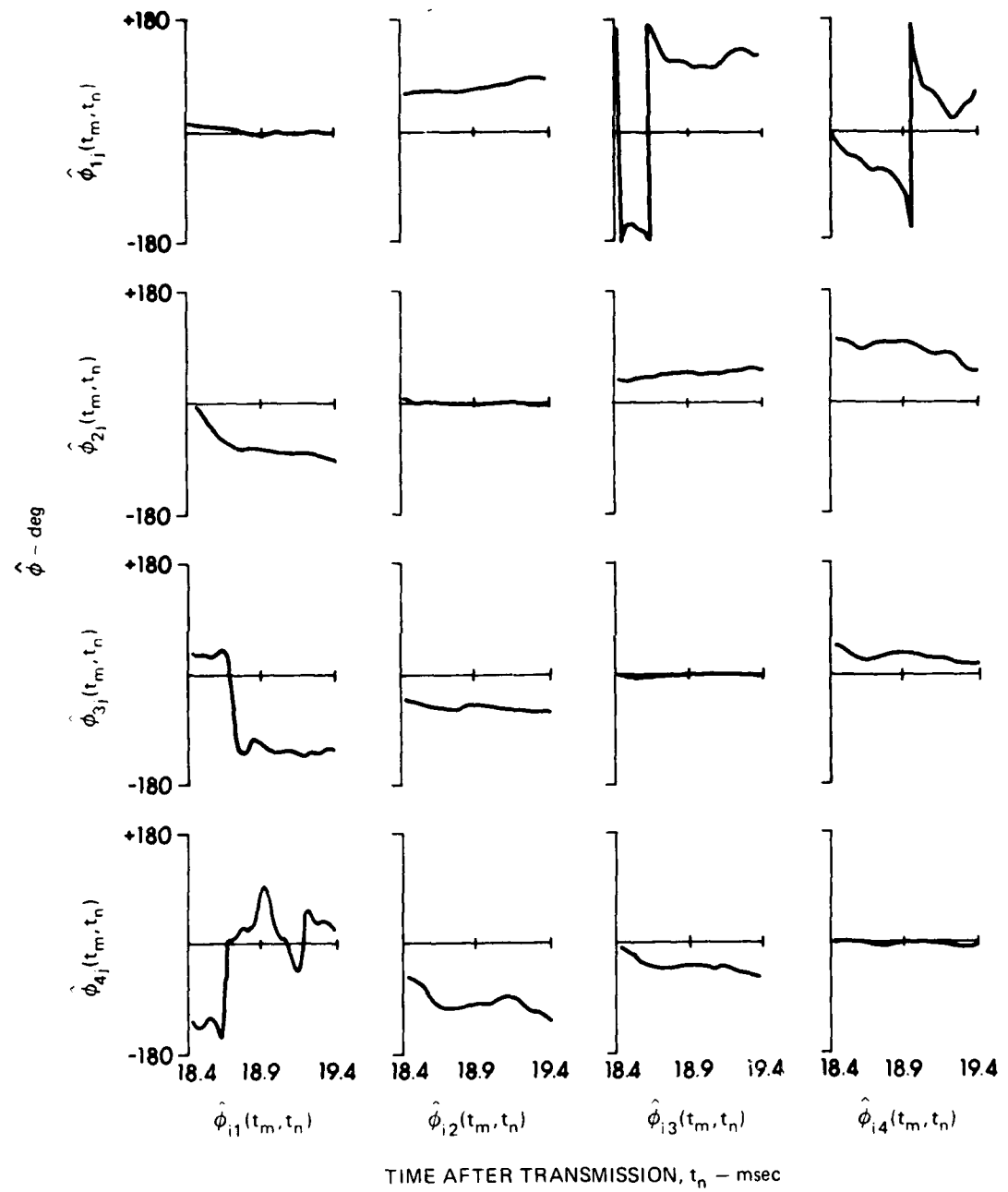


FIGURE 4.1  
ENVELOPES OF THE NORMALIZED COVARIANCE MATRIX  
(1 msec cw REVERBERATION AT  $t_m = 18.9$  msec AFTER TRANSMISSION)

ARL:UT  
AS-81-281  
MEF - GA  
3-11-81



**FIGURE 4.2**  
**PHASES OF THE COVARIANCE MATRIX**  
 (1 msec cw REVERBERATION AT  $t_m = 18.9$  msec AFTER TRANSMISSION)

ARL:UT  
AS-81-282  
MEF - GA  
3 - 11 - 81

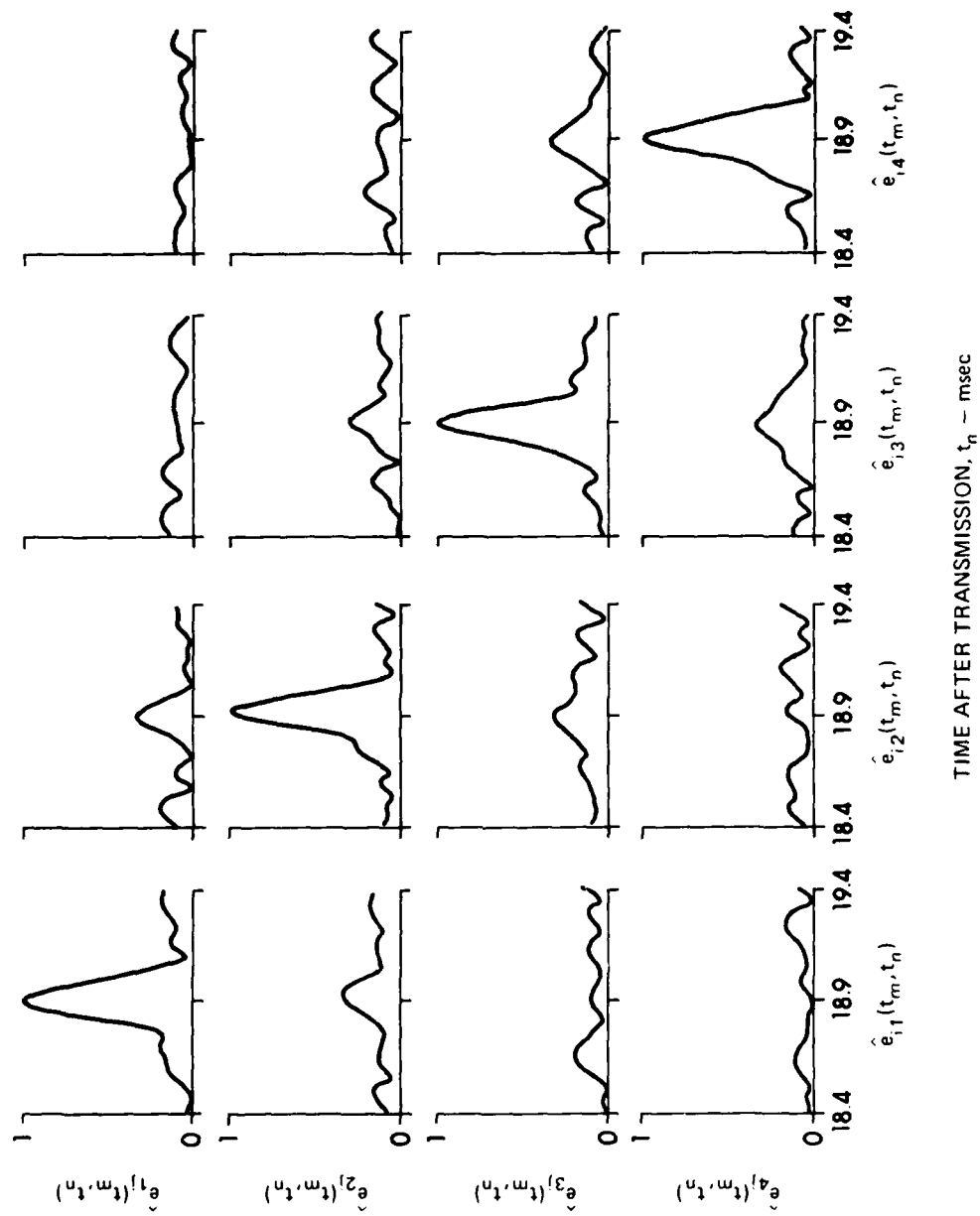
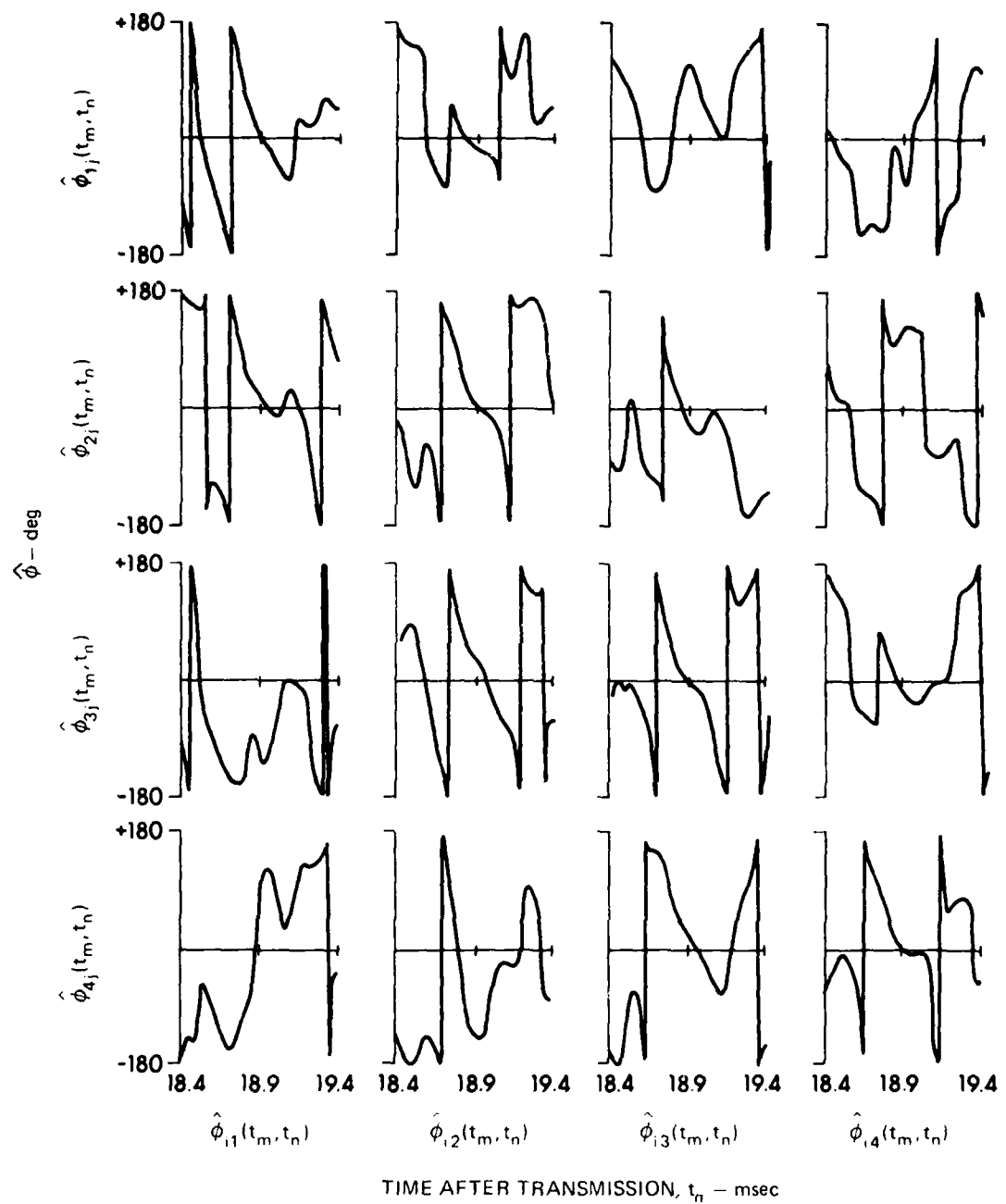


FIGURE 4.3  
ENVELOPES OF THE NORMALIZED COVARIANCE MATRIX  
(1 msec LFM REVERBERATION AT  $t_m = 18.9$  msec AFTER TRANSMISSION)

ARL:UT  
AS-81-283  
MEF-GA  
3-11-81



**FIGURE 4.4**  
**PHASES OF THE COVARIANCE MATRIX**  
 (1 msec LFM REVERBERATION AT  $t_m = 18.9$  msec AFTER TRANSMISSION)

ARL:UT  
AS-81-284  
MEF - GA  
3-11-81

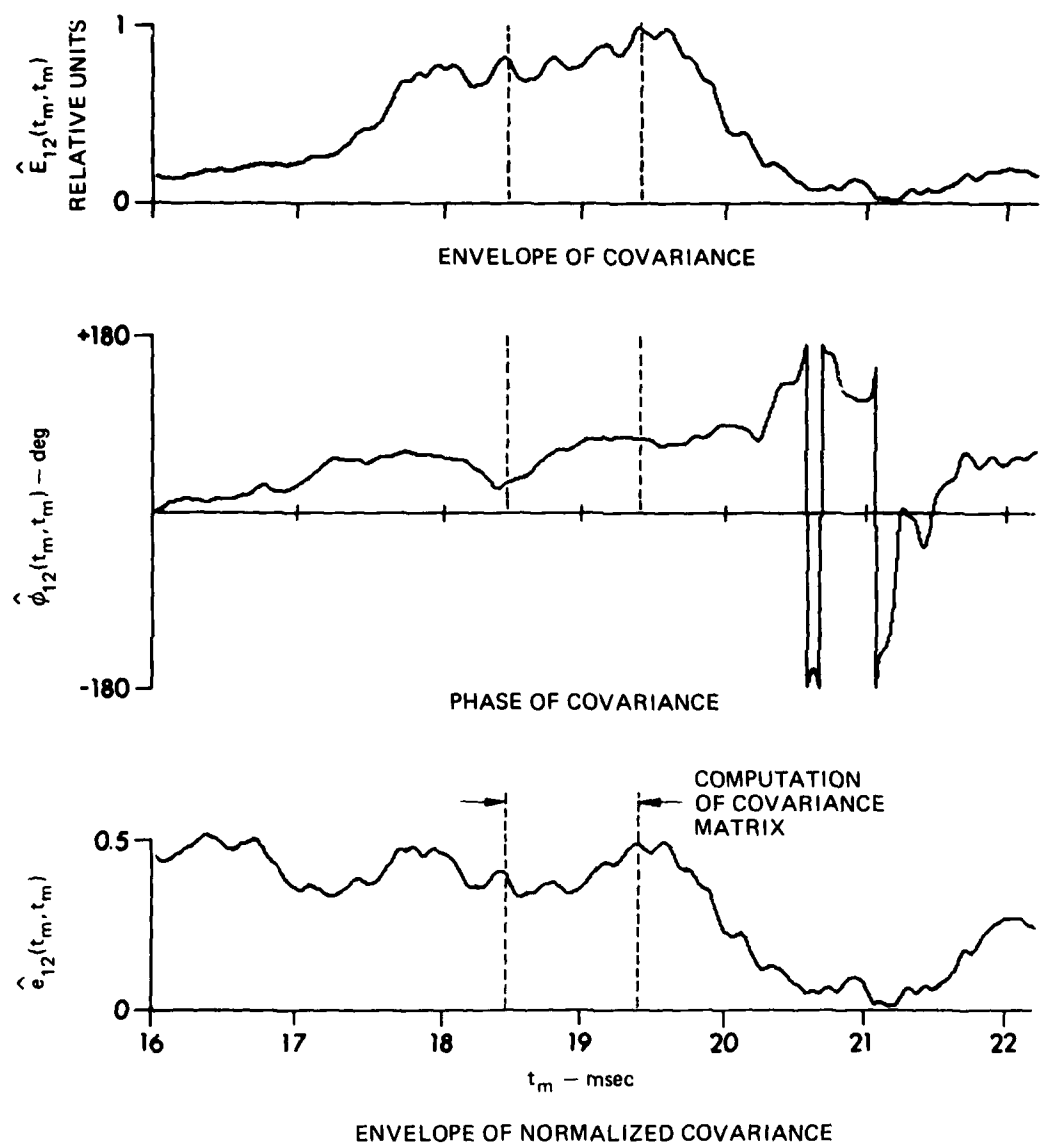


**FIGURE 4.5**  
**COVARIANCE BETWEEN ELEMENTS 1 AND 2**  
(1 msec cw REVERBERATION)

ARL:UT  
AS-81-285  
MEF - GA  
3-11-81

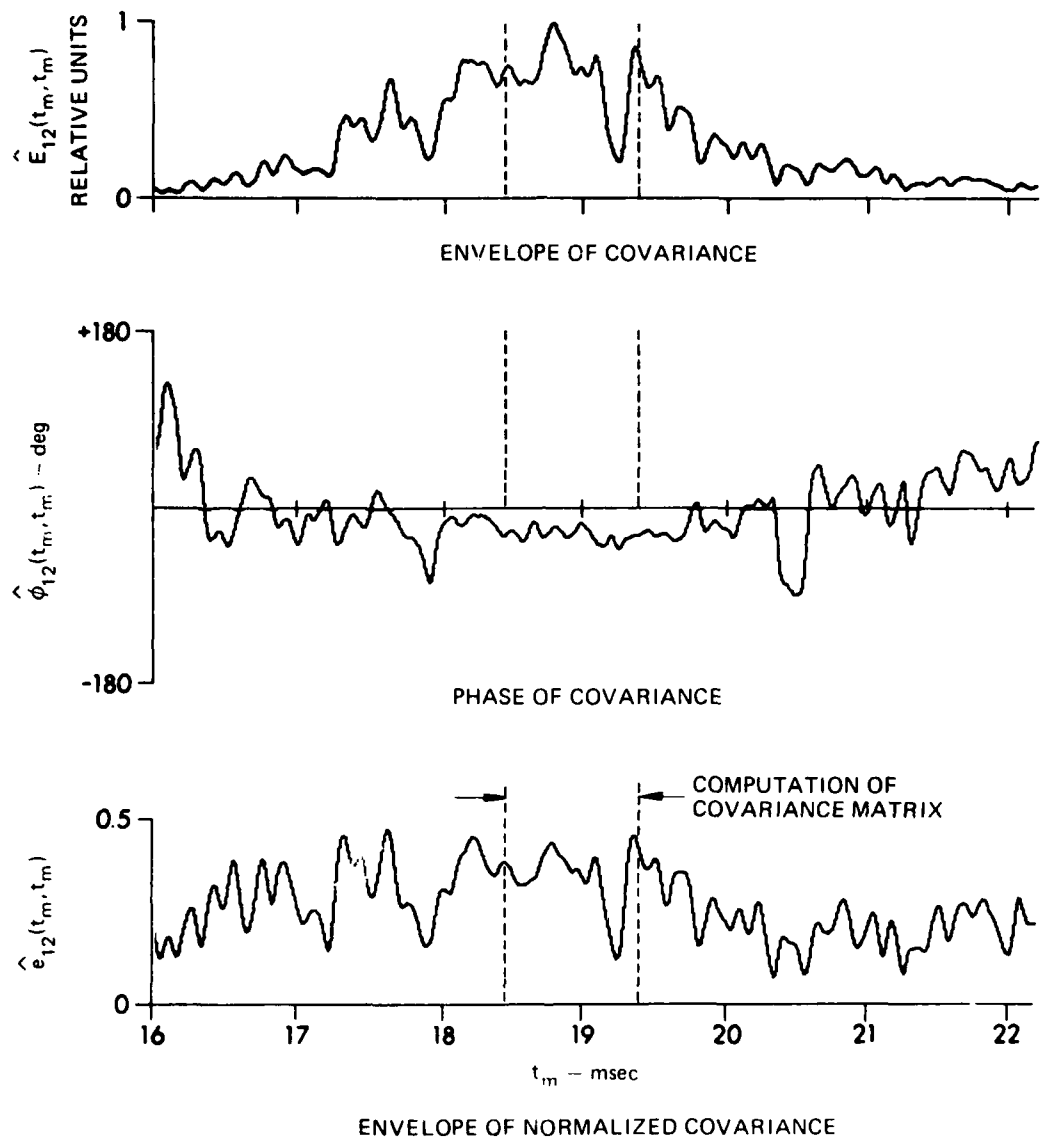


**FIGURE 4.6**  
**COVARIANCE BETWEEN ELEMENTS 1 AND 2**  
(1 msec LFM REVERBERATION)

ARL-UT  
AS-81-286  
MEF-GA  
3-11-81

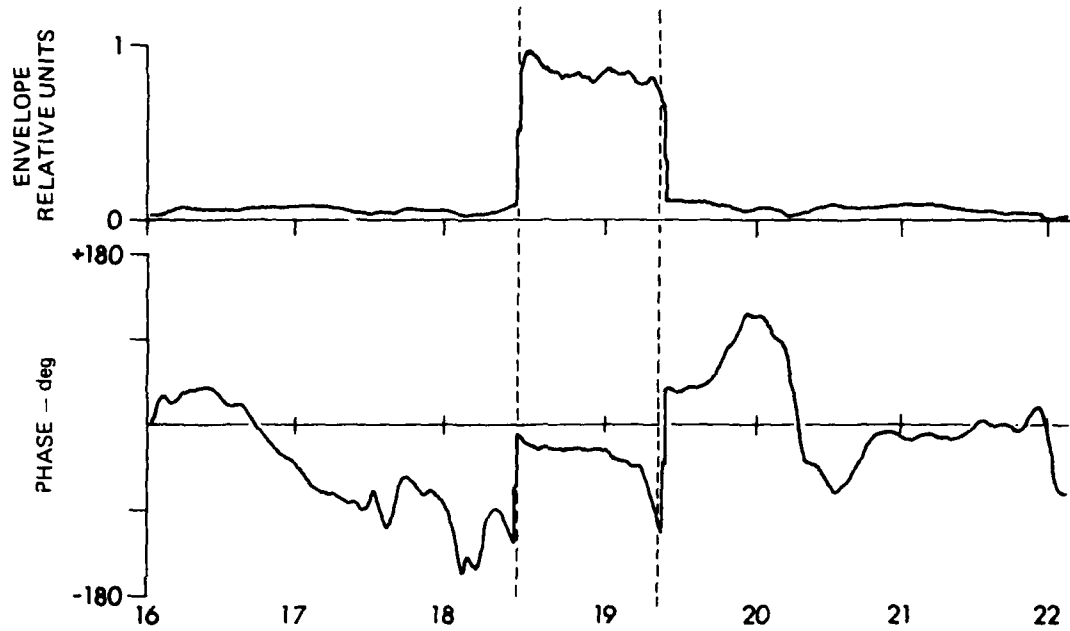
reverberation level than the other three channels, then this channel would have a more pronounced effect on the detection problem than the other three. Since this study is attempting to evaluate the effect of inter-channel covariance, rather than the obvious effect of having little or no noise on one channel, a multiplying factor was applied to all the returns from each channel so that the average noise level is the same as that for the channel with the lowest noise level. The average used for this purpose was the mean square value of all 320 samples from each of the events from a particular channel. This process was also performed on the signal echoes, although in that case there was only one return per channel.

### C. The Detection Problem

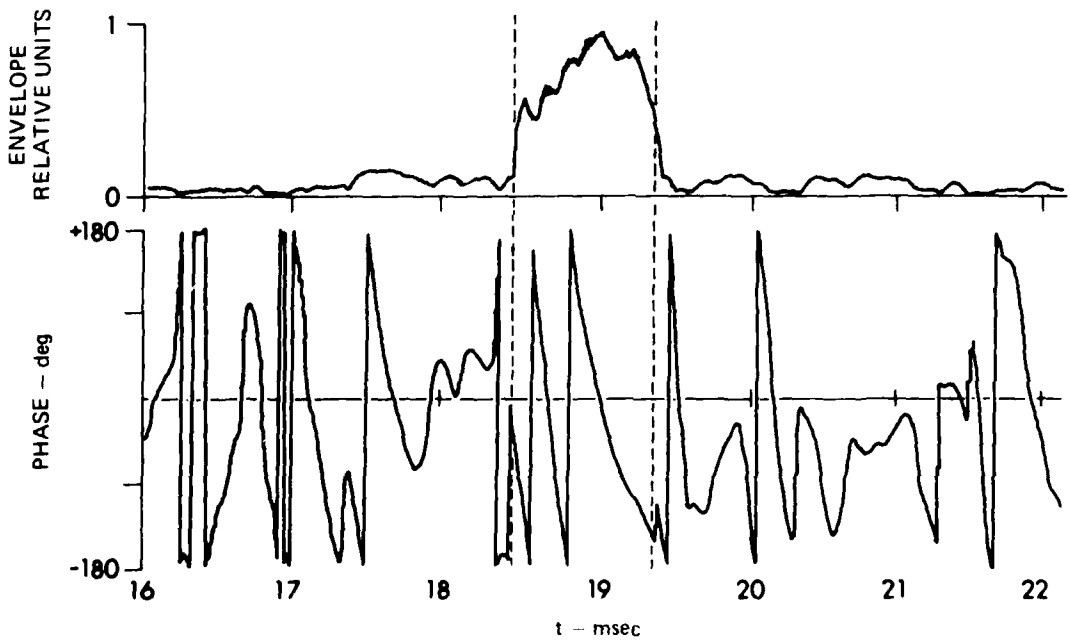
The detection problem considered here is studied by adding a known signal to a series of noise returns. The known signal consists of the echo from a styrofoam sphere measured in a high signal-to-noise environment. The noise returns consist of reverberation obtained by pointing the transmitter and receiver toward the surface as described in the previous chapter. To facilitate control of the signal-to-noise ratio when adding the signal to the noise returns, the signal samples were adjusted so that their mean square value was equal to that of the reverberation returns. Envelope plots of signal-plus-noise returns for channel one are shown in Fig. 4.7 for both the cw and LFM data. The dashed lines indicate the portion of the return which is under test by the detection process. In all cases considered in the detector evaluation, the S/N is much lower than the example in Fig. 4.7.

To evaluate the performance of the detector developed in Section II.C.2, both the predicted and the experimental ROC curves are presented. The predicted curve is found in the manner followed in Section II.C.3 except that under hypothesis  $H_1$ ,  $V=N+aS$ , where  $a=10^{**}(\text{SNR}/20)$ . With that assumption Eq. (2.12) becomes

$$\beta = 1 - \Phi\{\Phi^{-1}(1-\alpha) - a\sigma_\lambda\} \quad , \quad (4.5)$$



(a) 1 msec cw SIGNAL + REVERBERATION



(b) 1 msec LFM SIGNAL + REVERBERATION

**FIGURE 4.7**  
**EXAMPLE ENVELOPES AND PHASES OF SIGNAL + REVERBERATION**  
 (20 dB rms SIGNAL TO rms REVERBERATION)

ARL UT  
 AS-81-287  
 MEF - GA  
 3-11-81

where  $\sigma_{\lambda}^2 = \underline{S}^T \underline{K}^{-1} \underline{S}$  as before. The experimental performance is obtained by solving for the vector of filter coefficients  $\underline{B}$  (Eq. 2.6) and processing each of the reverberation returns. This processing consists of computing a test statistic  $\lambda$  by forming the scalar product of  $\underline{B}$  and  $\underline{N}$  for each member of the ensemble of reverberation returns. A histogram is made of the resulting test statistics

$$\lambda_{\gamma} = \underline{N}^T \underline{B} \quad \gamma = 1, \Gamma \quad ,$$

where  $\gamma$  is the event number mentioned earlier and  $\Gamma$  is the total number of events. This histogram is formed by dividing the range of  $\lambda$ , i.e.,  $(\lambda_{\max} - \lambda_{\min})$  into 20 bins and counting the number of  $\lambda$ 's which fall within each bin. The experimental density function under the noise-only hypothesis ( $H_0$ ) is

$$p_{\lambda/H_0}(i) = \frac{\text{number of hits in bin } i}{\Gamma} \quad .$$

When the signal-plus-noise returns are processed in a similar manner, the density function for  $\lambda$  under the signal-present hypothesis,  $p_{\lambda/H_1}(i)$ , is obtained. Alternatively,  $p_{\lambda/H_1}(i)$  may be obtained directly from  $p_{\lambda/H_0}(i)$  by observing that under  $H_1$

$$\lambda = (\underline{N} + a\underline{S})^T \underline{B} = \underline{N}^T \underline{B} + a \underline{S}^T \underline{B} \quad ,$$

and hence  $p_{\lambda/H_1}$  is merely  $p_{\lambda/H_0}$  shifted right by  $a \underline{S}^T \underline{B}$ . Points  $[(\alpha(j), \beta(j))]$  on the ROC curve are then computed by

$$\alpha(j) = \sum_{i \geq j} p_{\lambda/H_0}(i) \quad , \quad (4.6)$$

and

$$\beta(j) = \sum_{i \geq j} p_{\lambda/H_1}(i), \quad j = 1, 20 + \text{number of bins in } aS^T B. \quad (4.7)$$

Several comparisons are made in the following sections between the performance predicted theoretically by Eq. (4.5) and that measured experimentally by Eqs. (4.6) and (4.7).

#### D. Analysis of Results

To evaluate detector performance the system of linear equations indicated by Eq. (2.6) was solved for several different covariance matrices. This computation was performed on ARL:UT's CDC Cyber 171 computer using an algorithm titled LEQT2P from International Mathematical and Statistical Libraries.<sup>22</sup> When the size of the system became larger than 100, the linear system routine failed to obtain a solution. However, for all results presented in this study, the solutions were accurate to within 10 decimal digits. As an additional check on the validity of the results, the variance of the experimental  $\lambda$ 's was compared to that computed by Eq. (2.8). Since the covariance matrix  $K$  was computed from the same set of noise events that were used to test the detector, the two variances should be equal. This is true in all cases considered here.

##### 1. Effect of Input Signal-to-Noise Ratio

The first results to be presented are the optimum detector's performance for various input signal-to-noise ratios (S/N). Only one channel is considered and samples are taken according to Eqs. (2.14)-(2.16) with  $k=8$ , producing ten samples of each quadrature component during a 1 msec time interval. This represents sampling each quadrature component at the Nyquist rate since the data are essentially limited to a bandwidth of 10 kHz. Figures 4.8 and 4.9 represent the predicted and experimental performance of the optimum detector for the cw and LFM data, respectively. In both cases the experimental and predicted values agree

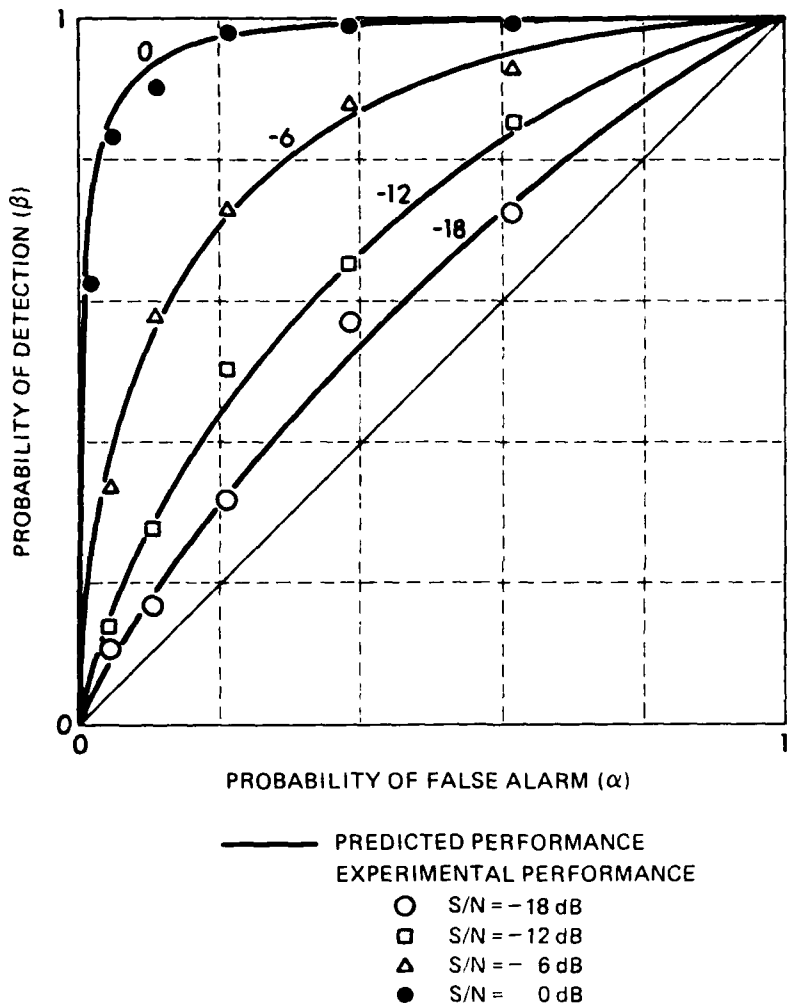
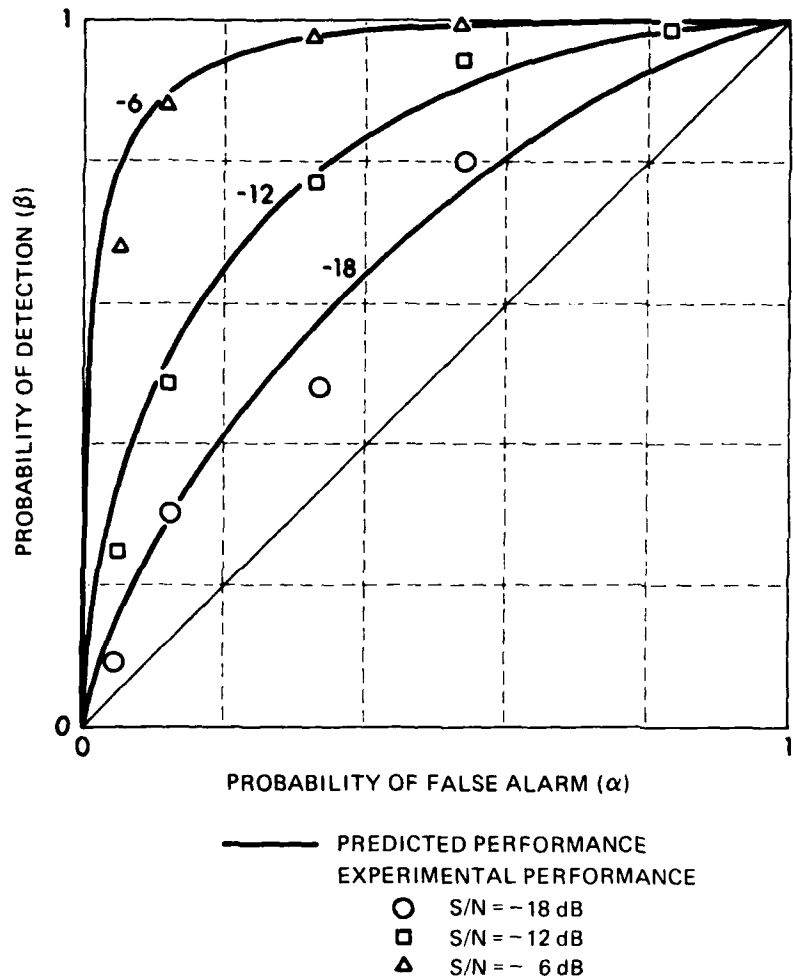


FIGURE 4.8  
**EXPERIMENTAL AND PREDICTED DETECTOR PERFORMANCE  
FOR VARIOUS INPUT SIGNAL-TO-NOISE RATIOS**  
(1 msec cw DATA, CHANNEL 1, SAMPLING PARAMETER  $k = 8$ )

ARL-UT  
AS-81-288  
MEF-GA  
3-11-81



**FIGURE 4.9**  
**EXPERIMENTAL AND PREDICTED DETECTOR PERFORMANCE**  
**FOR VARIOUS INPUT SIGNAL-TO-NOISE RATIOS**  
(1 msec LFM DATA, CHANNEL 1, SAMPLING PARAMETER  $k = 8$ )

ARL-UT  
AS-81-289  
MEF-GA  
3-11-81

rather closely. Also, note that the LFM detector is more powerful than the cw detector for the same S/N. This is generally the case when the transmitted pulse lengths are equal and is primarily due to the shorter correlation time of the LFM reverberation, i.e., the LFM covariance matrix is more nearly diagonal.

## 2. Effect of Sampling Frequency

Next the effect of sampling frequency is considered. With the input S/N fixed at -24 dB, several values of  $k$  were utilized in the detection problem. The results are shown in Figs. 4.10 and 4.11 for  $k=20, 10, 8, 4$ , and 2 for the single channel cw and LFM data sets. This range of  $k$  results in input vectors of lengths 8, 16, 20, 40, and 80. Again note the agreement between the experimental and predicted performance. Also, observe the pronounced improvement as the sampling frequency is increased. There is a large jump in improvement when  $k=2$ , i.e., the sampling frequency is 40 kHz per quadrature component. The close agreement between the predicted and experimental results is indicative that the phenomenon is not due to some computational error. These results demonstrate that sampling frequency is not a trivial concern in a study such as this one. Furthermore, these results expose the fallacy of a naive consideration of signal detection in a bandlimited environment. That is, in both the  $k=4$  and  $k=2$  cases, the samples are taken at a rate which exceeds the Nyquist frequency. Thus one might conjecture that in the  $k=4$  case (20 kHz per quadrature component) one could interpolate with the sampling expansion and thus reconstruct the additional samples that would be present in the  $k=2$  case (40 kHz per quadrature component). Then one might conclude that since the Neyman-Pearson detector optimally processes the data, the performance in the  $k=4$  case should be very close to the performance in the  $k=2$  case. However, as we have seen, this conjecture is not true. The interpolation error associated with the above reasoning is thus significant in this context.

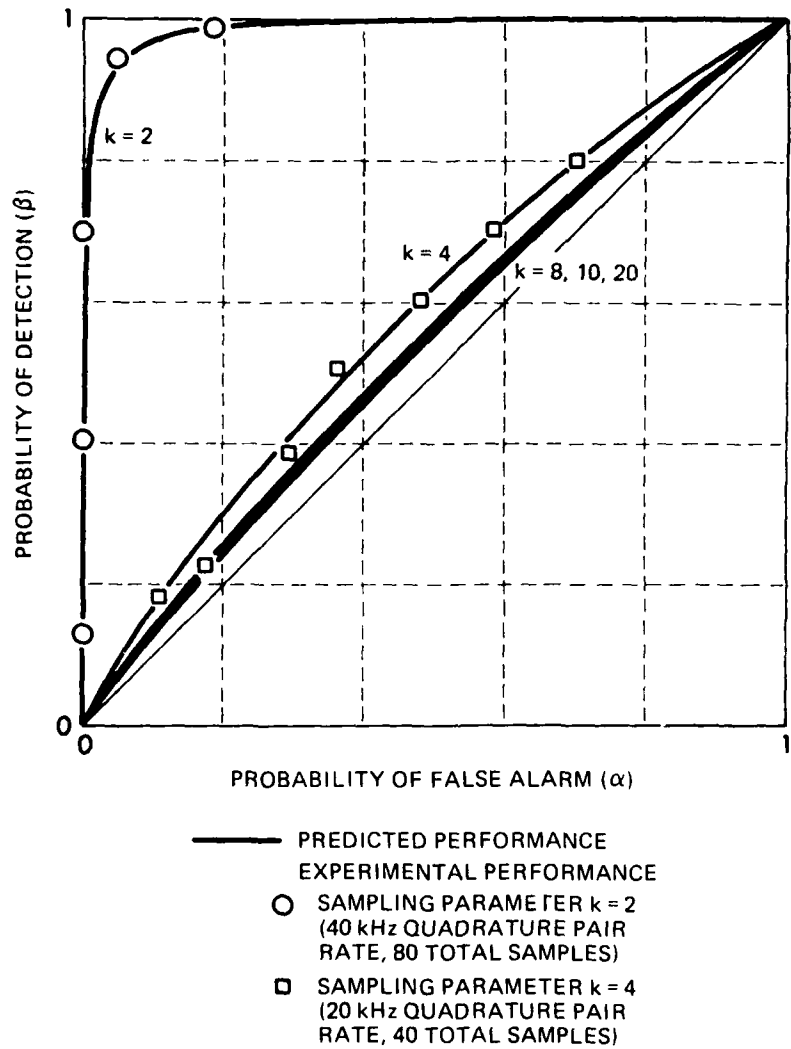


**FIGURE 4.10**  
**EFFECT OF SAMPLING PARAMETER  $k$**   
**ON DETECTOR PERFORMANCE**  
(1 msec cw DATA, CHANNEL 1, INPUT S/N = -24 dB)

ARL:UT  
AS-81-290  
MEF - GA  
3-11-81

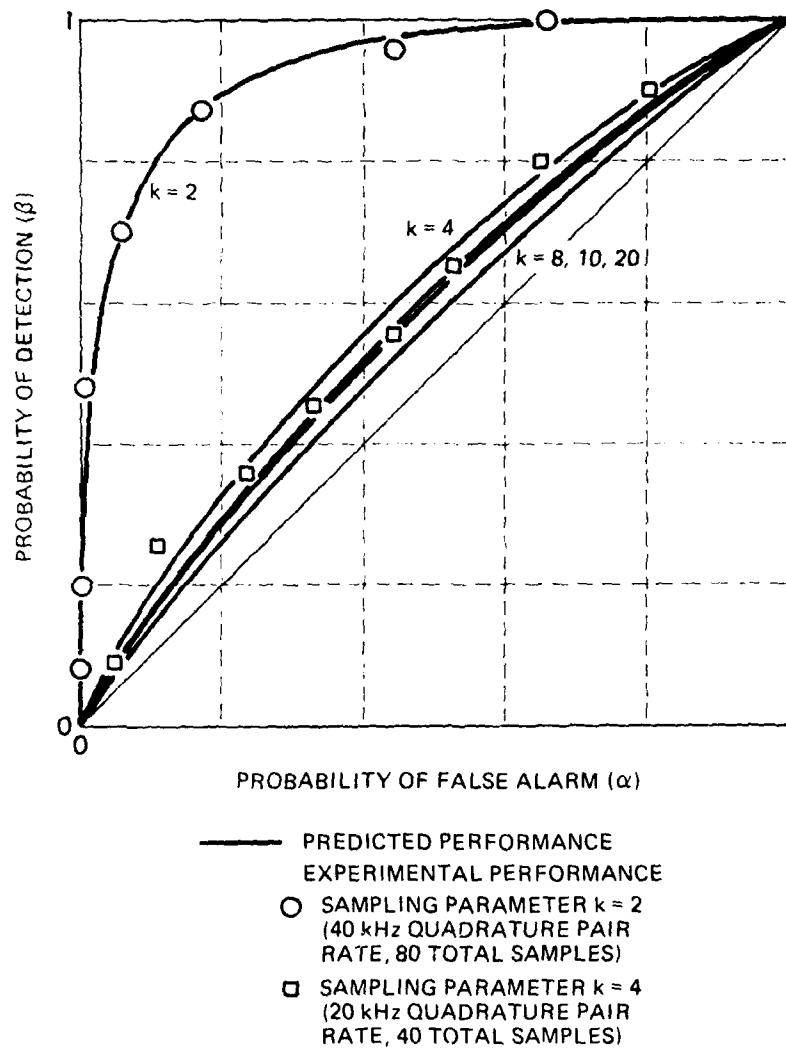


FIGURE 4.11  
EFFECT OF SAMPLING PARAMETER  $k$   
ON DETECTOR PERFORMANCE  
(1 msec LFM DATA, CHANNEL 1, INPUT S/N = -24 dB)

ARL:UT  
AS-81-291  
MEF-GA  
3-11-81

### 3. Multiple Channels

Most active sonars involve not just one element but an array of elements. The covariance matrix associated with such a multiple sensor system contains both spatial and temporal information about the noise processes on each element. The results described in this section relate to the optimum detector utilizing all this covariance information.

The input to the detector consists of four vectors  $\underline{v}_i$ ,  $i=1, 4$  as in Eq. (2.14) where each  $\underline{v}_i$  consists of samples according to Eqs. (2.14)-(2.16). From this point on the detector is evaluated as before in terms of  $\underline{B}$ ,  $\underline{K}$ , and  $\underline{S}$  except that  $\underline{B}$  and  $\underline{S}$  now represent groups of vectors and  $\hat{\underline{K}}$  is a matrix of submatrices. In other words, once  $\underline{B}$ ,  $\underline{K}$ , and  $\underline{S}$  are formed, they are treated exactly as they were in the single channel case.

Figures 4.12 and 4.13 demonstrate the performance improvement as the number of channels is increased from one to four. Here the  $S/N = -24$  dB and the sampling parameter  $k=8$ , resulting in a sampling rate of 10 kHz per quadrature component on each channel. As before the experimental points agree closely with the predicted curves.

### 4. Suboptimum Detectors - Multiple Channels

In the following presentation comparisons are made between the optimum detector and several simplified processors. The simplified processors are derived by making certain assumptions about the noise processes which result in a simpler covariance matrix. To predict the performance of these suboptimum detectors, the method of Section II.C.3 is pursued using the assumed form of the covariance matrix. Let

$$\hat{\underline{B}} = \hat{\underline{K}}^{-1} \underline{S} \quad ,$$

where  $\hat{\underline{K}}$  is the assumed covariance matrix and  $\hat{\underline{B}}$  is the array of coefficients

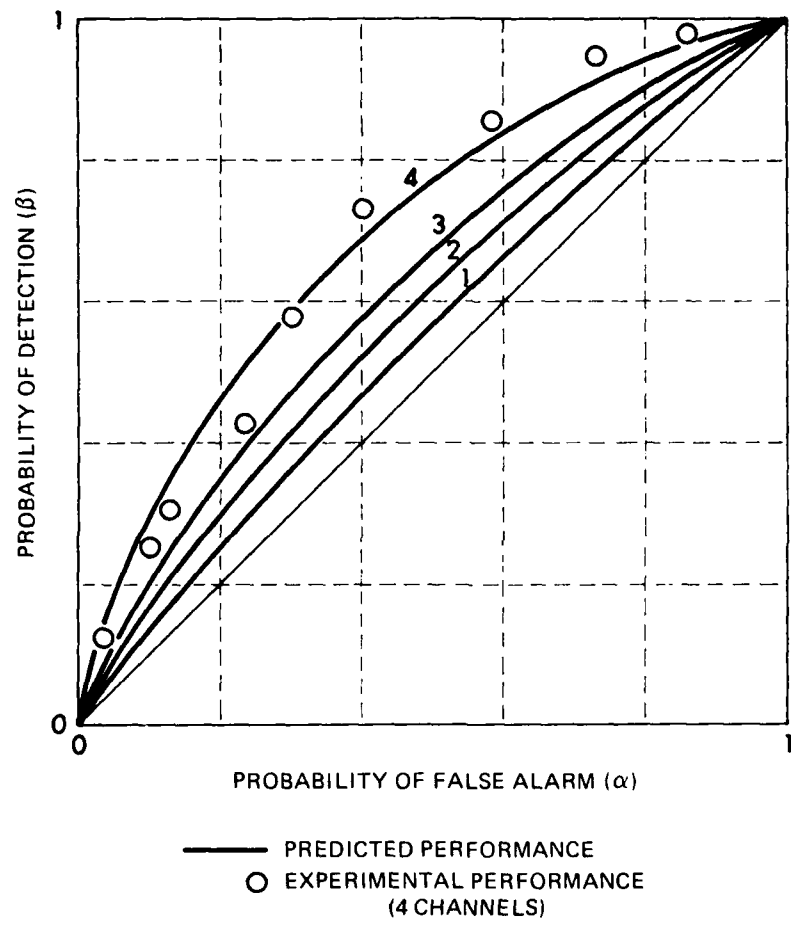


**FIGURE 4.12**  
**DETECTOR PERFORMANCE WITH NUMBER**  
**OF CHANNELS AS A PARAMETER**  
 (1 msec cw DATA, SAMPLING PARAMETER  $k = 8$ ,  
 INPUT S/N = -24 dB)

ARL:UT  
 AS-81-292  
 MEF - GA  
 3-11-81

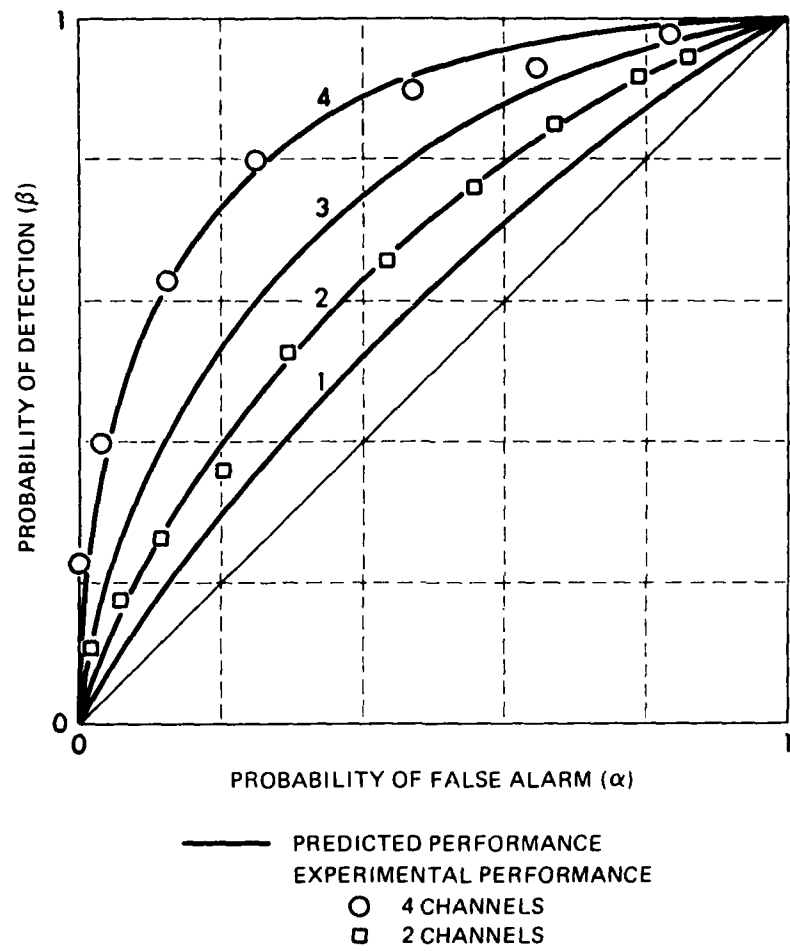


FIGURE 4.13  
DETECTOR PERFORMANCE WITH NUMBER  
OF CHANNELS AS A PARAMETER  
(1 msec LFM DATA, SAMPLING PARAMETER  $k = 8$ ,  
INPUT S/N = -24 dB)

ARL:UT  
AS-81-293  
MEF - GA  
3-11-81

for the associated suboptimum detector. The test statistic produced by processing the data with  $\hat{\underline{B}}$  is

$$\hat{\lambda} = \underline{V}^T \hat{\underline{B}} \quad ,$$

with mean value

$$E\{\hat{\lambda}\} = E\{\underline{V}^T\}\hat{\underline{B}}$$

and variance

$$\begin{aligned} \sigma_{\hat{\lambda}}^2 &= E\{[\hat{\lambda} - E(\hat{\lambda})]^2\} = E\left\{[(\underline{V} - E\{\underline{V}\})^T \underline{K} \hat{\underline{B}}]^2\right\} \\ &= \hat{\underline{B}}^T \underline{K} \hat{\underline{B}} \quad . \end{aligned}$$

As before the matrix  $\underline{K}$  represents the true covariance of the noise process. The means under the null and alternate hypotheses are

$$H_0: \hat{\underline{m}}_0 = E_0\{\hat{\lambda}\} = \underline{M}^T \hat{\underline{B}}, \text{ and}$$

$$H_1: \hat{\underline{m}}_1 = E_1\{\hat{\lambda}\} = E_1\{\underline{N}^T \hat{\underline{B}} + a \underline{S}^T \hat{\underline{B}}\}$$

$$= \underline{M}^T \hat{\underline{B}} + a \underline{S}^T \hat{\underline{B}}$$

$$= \hat{\underline{m}}_0 + a \underline{S}^T \hat{\underline{B}} \quad .$$

The performance is determined again as in Section II.C.3 to be

$$\beta = 1 - \phi \left\{ \frac{\hat{\underline{m}}_0 + \sigma_{\hat{\lambda}} \phi^{-1}(1-\alpha) - \hat{\underline{m}}_1}{\sigma_{\hat{\lambda}}} \right\}$$

$$\beta = 1 - \Phi \left\{ \Phi^{-1}(1-\alpha) - \frac{aS^T \tilde{B}}{\sqrt{\tilde{S}^T \tilde{K} \tilde{B}}} \right\} \quad . \quad (4.8)$$

Note that, if  $\tilde{B} = \underline{K}^{-1} \underline{S}$ , then Eq. (4.8) simplifies to Eq. (2.12) as it should. Also note that the performance is completely determined (for a given S/N) by

$$d^2 \triangleq \sqrt{\frac{S^T \tilde{B}}{\underline{K}^T \tilde{K} \tilde{B}}} \quad , \quad (4.9)$$

commonly referred to as the detectability index.<sup>23</sup> The performance of several suboptimum detectors is presented below by tabulating the values of  $d^2$  assuming  $\underline{K} = \hat{K}$ .

CASE I: Assume that the noise process is wide sense stationary over the 1 msec observation interval. In that case the covariance matrix elements  $\hat{K}_{ij}(t_m, t_n)$  would only be functions of  $t_n - t_m$  given i and j. To determine the effect of this assumption,  $\tilde{K}$  is taken to be  $\underline{K}$  with each element replaced by the average along the diagonal within its submatrix, i.e.,

$$\tilde{K}_{ij}(t_n - t_m) = \begin{cases} \frac{1}{N + n - m} \sum_{k=1}^{N+n-m} \hat{K}_{ij}(m-n+k, k), & m - n \geq 0 \\ \frac{1}{N - n + m} \sum_{k=1}^{N-n+m} \hat{K}_{ij}(k, n-m+k), & m - n < 0 \end{cases} .$$

This operation produces a matrix which has the same general form as the true covariance but would appear to have come from a wide sense stationary noise process.

CASE II: Assume the process is independent in time. Here  $\hat{K}$  is formed by setting to zero all elements of  $\hat{K}$  except those along each submatrix diagonal (including the main diagonal).

CASE III: Assume the process is independent in space. In this case  $\hat{K}$  consists of the autocovariance submatrices of  $\hat{K}$ .

CASE IV: Assume cases I-III. Here  $\hat{K}$  is a diagonal matrix with all diagonal elements equal to the average of the diagonal elements of  $\hat{K}$  and all other elements are zero. This case represents the assumption most typically made in the design of signal processors in many modern sonars. This assumption leads to the simple matched filter (see Section II.C.2) because the filter coefficients are equal to the signal samples within a scale factor (assuming equal variance on all channels).

Table II presents  $d^2$  for the cw and LFM data sets. Included are the optimum detector and CASES I-IV for sampling parameter  $k=8$ . When the number of channels in the cw data is greater than one, the linear equation solving routine is unable to reach a solution for the CASE I problem. In all cases presented in Table II the experimental performance agreed closely with the performance predicted by Eq. (4.8).

The CASE I results are especially significant in that they represent a detection performance of a processor utilizing a more realistically obtainable covariance matrix. A similar matrix might be obtained from a theoretical model<sup>8</sup> which might accurately reflect the overall matrix structure. An actual covariance matrix would seldom be available. CASE I is also significant because the wide sense stationary assumption leads to a simpler processor, derived by Adams and Nolte,<sup>23</sup> requiring the inversion of smaller matrices with an order equal to the number of channels. Thus, the CASE I results are more nearly representative of those which might be obtained using a predicted covariance matrix and a simplified processor structure.

TABLE II  
COMPARISON OF DETECTOR PERFORMANCE ( $d^2$ ) FOR  
OPTIMUM AND SIMPLIFIED PROCESSORS

Data Type	Number of Channels	Optimum	CASE I	CASE II	CASE III	CASE IV
			(Stationary)	(Independent In Time)	(Independent In Time)	(CASES I-III)
CW	1	2.76	2.62	1.77	2.76	1.75
	2	4.92	No Solution	2.09	4.09	2.06
	3	7.14	No Solution	2.59	4.86	2.46
	4	11.8	No Solution	3.04	6.07	2.92
LFM	1	4.87	4.14	3.71	4.87	3.66
	2	9.29	7.26	6.16	8.30	5.87
	3	14.7	10.0	8.28	10.3	7.89
	4	23.3	10.3	8.58	10.9	8.66

Sampling Parameter  $k=8$ , Sampling Frequency = 10 kHz per quadrature component

## 5. Suboptimum Detectors - Single Channel

Consideration of CASES I and II for the single channel problem also yields interesting results. Table III presents the detectability indices for CASES I and II, I and II combined, and the optimum detector for the cw and LFM data. The sampling parameter  $k$  is varied from 20 to 2 corresponding to sample frequencies of 2.5-40 kHz. For both data sets the linear system's routine failed to reach a solution for CASE I when  $k=2$  and 4. Observe that simplified processors do not exhibit the pronounced improvement with sample frequency apparent in the optimum detector results. The fact that CASE II and the combination of CASES I and II are very nearly in agreement indicates that the diagonal elements of the covariance matrix do not vary significantly over the 1 msec time interval. In other words, the variance does not change enough over the observation interval to significantly affect the performance of the simplest detector (CASES I and II combined).

## 6. Detection Probability versus Signal-to-Noise Ratio

The degree of improvement of the optimum over any of the simplified processors may also be observed by considering the performance as a function of S/N. For notational convenience Eqs. (4.8) and (4.9) are combined to produce

$$\beta = 1 - \Phi\{\Phi^{-1}(1-\alpha) - ad^2\} \quad , \quad (4.10)$$

where again  $a=10^{**}(\text{SNR}/20)$ .

In Fig. 4.14  $\beta$  versus S/N is plotted with  $\alpha=0.1$  for the 4-channel cw data. Both the optimum detector and the simple matched filter (CASE IV) results are shown allowing comparison of their performance. At the 50% detection probability the optimum detector provides approximately a 13 dB improvement over the simple matched filter.

TABLE III  
COMPARISON OF SINGLE CHANNEL DETECTOR PERFORMANCE ( $d^2$ ) FOR  
OPTIMUM AND SIMPLIFIED PROCESSORS

Data Type	Sampling Parameter k	Sampling Frequency (kHz) (Pair Rate)	Optimum	CASE I		CASE II (Independent)	CASES I and II
				(Stationary)	(Independent)		
1.0 msec cw	20	2.5	2.11	2.03	1.75	1.73	
	10	5	2.52	2.43	1.76	1.75	
	8	10	2.76	2.62	1.77	1.75	
	4	20	4.87	No Solution	1.78	1.77	
	2	40	49.8	No Solution	1.79	1.77	
	20	2.5	3.12	3.01	3.04	2.96	
	10	5	4.43	3.94	3.67	3.64	
	8	10	4.87	4.14	3.71	3.66	
1.0 msec LTM	4	20	6.21	No Solution	3.67	3.64	
	2	40	33.14	No Solution	3.67	3.63	

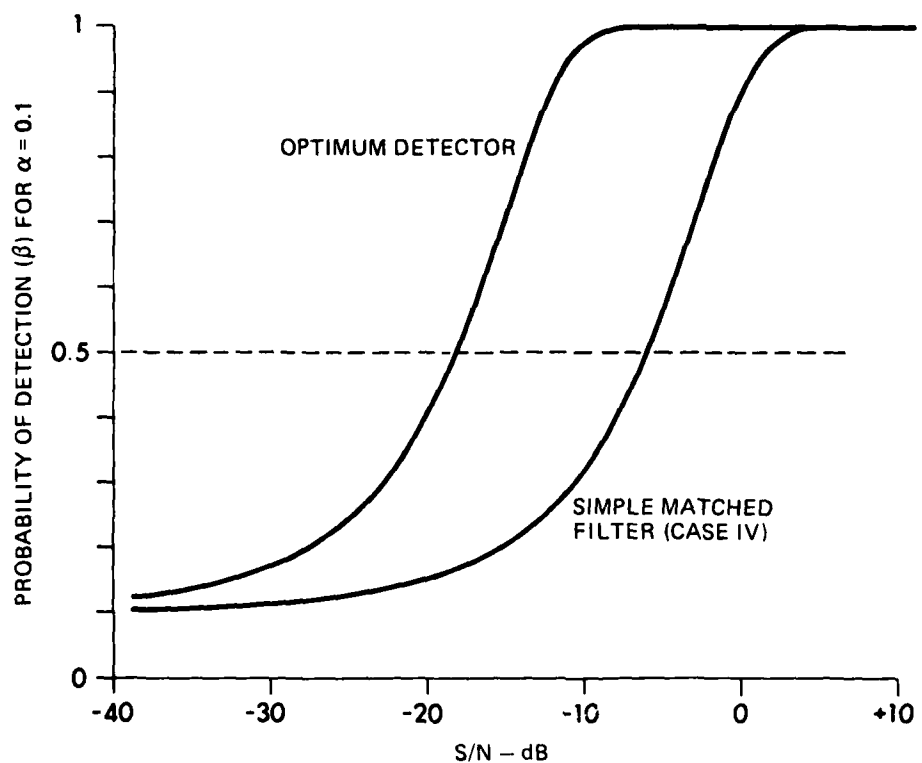


**FIGURE 4.14**  
**COMPARISON OF OPTIMUM AND SUBOPTIMUM DETECTOR**  
**PERFORMANCES FOR A 0.1 FALSE ALARM RATE**  
 (1 msec cw DATA, 4 CHANNELS, SAMPLING PARAMETER  $k = 8$ )

ARL:UT  
 AS-81-294  
 MEF - GA  
 3 - 11 - 81

Figure 4.15 presents similar results for the LFM data with the addition of the CASE I performance. Here the optimum detector provides an approximate 8 dB improvement over the simple matched filter. The improvement is less for the LFM data than for the cw because the LFM noise process is more nearly independent (see Figs. 4.1 and 4.3).

The wide sense stationary (CASE I) detector results shown in Fig. 4.15 represent the degree of improvement that might be obtained by considering a reasonably close facsimile of the actual covariance matrix. However, the improvement over the simple matched filter is relatively modest compared to the improvement the optimum system provides. The CASE I improvement would most likely be greater for the cw data; however, the routine failed to obtain a solution in that situation. In any case, these results again indicate the sensitivity of the detector to the actual elements of the covariance matrix.

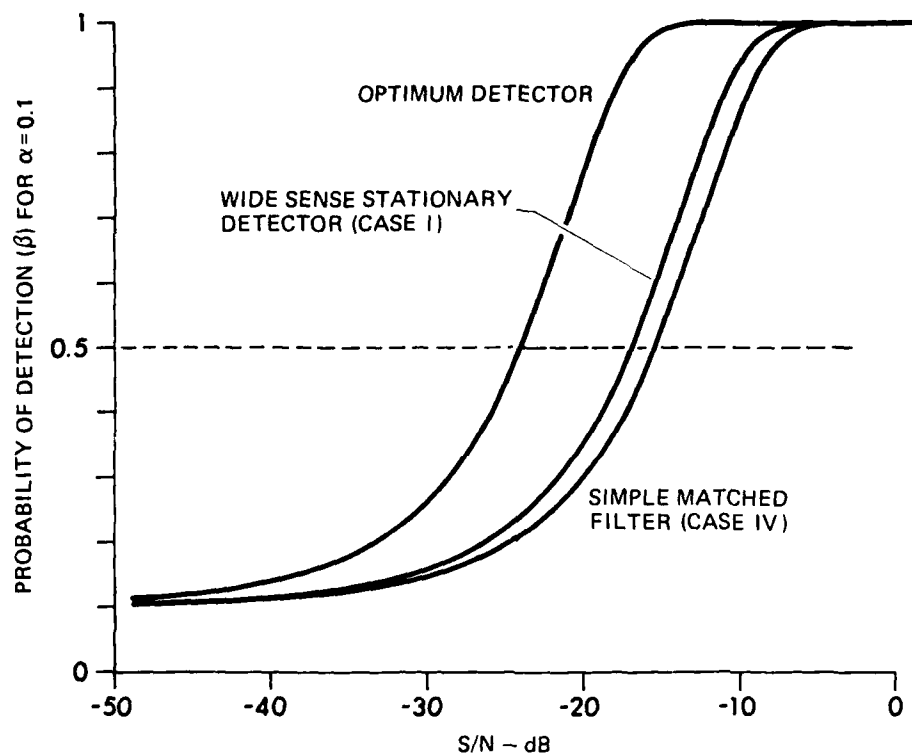


FIGURE 4.15  
 COMPARISON OF OPTIMUM AND SUBOPTIMUM DETECTOR  
 PERFORMANCES FOR A 0.1 FALSE ALARM RATE  
 (1 msec LFM DATA, 4 CHANNELS, SAMPLING PARAMETER  $k = 8$ )

ARL:UT  
 AS-81-295  
 MEF - GA  
 3-17-81

## V. CONCLUSIONS AND RECOMMENDATIONS

In this study several aspects of the discrete time Neyman-Pearson optimal detector have been investigated using experimental acoustic data. The problem considered is that of detecting a known signal from an active sonar operating in a reverberant environment. The noise background consists of sonar returns obtained by directing a transmitter and receiver toward the wind driven surface of a freshwater lake. High signal-to-noise ratio echoes from a styrofoam sphere provide the known signal. For both the echoes and reverberation, signals from four elements of a line array were digitized for analysis. In this manner both spatial and temporal aspects of the detection process were studied. The two types of sonar transmissions employed are a 1.0 msec pulsed continuous wave signal with a carrier frequency of 80 kHz and a 1.0 msec pulsed linear frequency modulated signal with a 10 kHz sweep centered at 80 kHz. Thus, this investigation consists of evaluating a well known (but not often employed) signal processing technique in a particular application.

The detection problem addressed in this study is a very special case of the general detection problem encountered by designers of active sonar systems. Generally this problem consists of detecting a contact of unknown location given a series of observations, i.e., multiple transmissions. Furthermore, the contact echo structure exhibits a certain amount of randomness independent of the noise background. In this study both the form and location of the signal are known precisely when the signal is present. For this reason only a fixed time interval is processed. Signal plus noise events are created by adding samples from the echoes to samples of the reverberation returns at specified signal-to-noise ratios. The reverberation is modeled as a Gaussian random process with a known covariance matrix. For the experimental detector evaluation, this matrix is computed by averaging over an ensemble of approximately

100 reverberation events. This matrix is employed by a likelihood ratio detector to process these same 100 returns.

While the detection problem considered here is specific in nature, it allows several aspects to be studied under closely controlled circumstances. These aspects include: (1) performance versus input signal-to-noise ratio, (2) effect of sampling frequency, (3) type of transmission, and (4) number of channels. In each case comparisons are made between predicted performance and that obtained experimentally by processing the 100 reverberation returns with and without the signal added. In all cases the theoretical and experimental estimates agreed rather closely. Comparisons are also made between the optimum detector's performance and that of several simplified processors. These simplified detectors are derived by making certain assumptions about the covariance matrix. Specifically the cases considered include assuming the noise process is: (1) wide sense stationary, (2) uncorrelated in space but correlated in time, (3) uncorrelated in time but correlated in space, and (4) uncorrelated in both space and time.

The results of this study are as follows:

1. An automatic method of alignment of multichannel data digitized from an analog tape recorder was developed. The results indicate that in all cases the data were aligned by this method to within one sample time.
2. Experimental detector performance agreed very closely with theoretical predictions in all cases. Thus, the detection performance may be predicted reliably from consideration of the covariance matrix.
3. Generally the detection performance for the LFM data was approximately 6 dB better than it was for the cw data. In other words the LFM performance was the same as the cw performance when the cw data's input signal-to-noise ratio was 6 dB higher than that for the LFM data.
4. Detection performance for both the cw and LFM data exhibits a definite improvement as the sampling frequency (and number of samples, since a fixed time interval is considered) is increased. While the author feels this result is rather inconclusive, it does indicate that

sampling frequency is a significant factor in the detector performance. The simple matched filter showed no improvement with increased sampling frequency.

5. Using all four channels the optimum detector provided the following improvement over a simple matched filter:

- (1) 13 dB for the 1.0 msec cw data, and
- (2) 8 dB for the 1.0 msec LFM data.

6. As the number of channels is increased, the improvement is more significant for the optimum detector than for the simple matched filters.

7. For the LFM data, approximating the covariance matrix in the optimum detector by one with similar form yields only a 3 dB performance improvement (see Fig. 4.15) over the simple matched filter. This improvement is modest compared to 8 dB obtained by employing the exact covariance matrix. Corresponding results for the cw data are not available due to computational difficulties.

This study might be improved or expanded by considering the following recommendations.

1. A larger ensemble of reverberation returns might be obtained and the covariance matrix estimated from one half of the ensemble could be used to process data from the other half.

2. By recording an ensemble of target echoes, the more general problem of detecting a random signal might be investigated.

3. The bearing sensitivity of the detector could be studied by changing the apparent received angle of the known signal.

4. The covariance matrix might be predicted from a theoretical model of the reverberation process. Thus the performance of the detector employing this matrix could be determined.

5. In an effort to understand the unusually high performance in the single channel, high sample rate example (Figs. 4.10 and 4.11), the performance could be determined as a function of the number of diagonals retained in the detector's assumed covariance matrix. In other words all matrix elements farther away from the principal diagonal than  $n$  diagonals could be set to zero and the performance could be measured as a function of  $n$ .

6. A solution for the performance of the wide sense stationary detector (CASE I) could be obtained for the cw data. This would involve modifying the linear equation solving routine used in this study.

APPENDIX

COMPUTATIONAL PROCEDURE FOR COMPUTING THE  
CROSSCORRELATION ENVELOPE USED FOR ALIGNMENT OF DATA SEQUENCES

The following discussion describes the computational procedure used to align data from different pings and channels and is taken primarily from Ref. 19.

Consider two narrowband functions,

$$f_1(t) = A_1(t) \cos\{\omega_0 t + \phi_1(t)\} ,$$

and

$$f_2(t) = A_2(t) \cos\{\omega_0 t + \phi_2(t)\} ,$$

where  $A_i(t)$  and  $\phi_i(t)$  are the slowly varying (with respect to  $\cos\omega_0 t$ ) amplitude and phase functions of  $f_i(t)$ ,  $\omega_0 = 2\pi f_0$ , and  $f_0$  is the center frequency. In quadrature form  $f_1$  and  $f_2$  are given by

$$f_1(t) = X_1(t) \cos\omega_0 t + Y_1(t) \sin\omega_0 t , \quad (1a)$$

and

$$f_2(t) = X_2(t) \cos\omega_0 t + Y_2(t) \sin\omega_0 t , \quad (1b)$$

where

$$X_i(t) = A_i(t) \cos\phi_i(t) ,$$

and

$$Y_i(t) = -A_i(t) \sin\phi_i(t) .$$

The crosscorrelation of  $f_1$  and  $f_2$  is given by

$$R_{12}(\tau) = f_1(t)*f_2(t) \stackrel{\Delta}{=} \int_{-\infty}^{+\infty} f_1(t)f_2(t+\tau)dt \quad . \quad (2)$$

Inserting Eqs. (1a) and (1b) in Eq. (2) yields

$$R_{12}(\tau) = X_{R_{12}}(\tau) \cos\omega_0\tau + Y_{R_{12}}(\tau) \sin\omega_0\tau \quad , \quad (3)$$

where

$$X_{R_{12}}(\tau) = 1/2\{X_1(t)*X_2(t) + Y_1(t)*Y_2(t)\} \quad (4a)$$

and

$$Y_{R_{12}}(\tau) = 1/2\{X_1(t)*Y_2(t) - X_2(t)*Y_1(t)\} \quad . \quad (4b)$$

Actually there are additional terms in Eq. (4) of the form  $(X_1(t) \cos 2\omega_0 t * X_2(t))$  which are found to be zero by the convolution theorem.

To compute the crosscorrelation between two low pass functions such as  $X_1(t)*X_2(t)$ , the interpolatory representation of this integral is used and is given by<sup>24</sup>

$$R'(ma) = 2a^2 W \sum_{n=1}^{\infty} X_1(na) X_2^*([m+n]a) \quad , \quad (5)$$

where  $W$  is the narrower bandwidth of the two signals and  $a$  is the sampling period, which is less than or equal to  $1/(2W)$ . Since the actual functions  $X_1$  and  $X_2$  are of finite duration, i.e.,  $X_1(na)=0$ ,  $n>N$  (where  $N$  is the number of samples in the finite interval), Eq. (5) reduces to

---

\*Strictly speaking, this statement violates the bandlimited assumption; however, in practice Eq. (6) is a good approximation.

$$R'(ma) = 2a^2 W \sum_{n=1}^N X_1(na) X_2([m+n]a) . \quad (6)$$

The envelope function of  $R_{12}$  is computed in the usual manner by

$$E_{12}(ma) = \sqrt{X_{R_{12}}^2(ma) + Y_{R_{12}}^2(ma)} . \quad (7)$$

Normalizing the crosscorrelation function is useful in that it provides a ready indication of problems in the data, i.e., when two similar functions are closely aligned the normalized value will be near unity. This function is given by

$$\rho_{12}(ma) = \frac{R_{12}(ma)}{\sqrt{R_{11}(0) R_{22}(0)}}$$

and the envelope of  $\rho_{12}$  by

$$e_{12}(ma) = \frac{E_{12}(ma)}{\sqrt{R_{11}(0) R_{22}(0)}} . \quad (8)$$

Combining Eqs. (4), (6), (7), and (8) yields

$$\begin{aligned} e_{12}^2(ma) &= \left\{ \left[ \sum_{n=1}^N X_1(na) X_2([m+n]a) + \sum_{n=1}^N Y_1(na) Y_2([m+n]a) \right]^2 \right. \\ &+ \left. \left[ \sum_{n=1}^N X_1(na) Y_2([m+n]a) - \sum_{n=1}^N X_2(na) Y_1([m+n]a) \right]^2 \right\} \\ &: \left\{ \left[ \sum_{n=1}^N X_{11}^2(na) + Y_{11}^2(na) \right] \left[ \sum_{n=1}^N X_{22}^2(na) + Y_{22}^2(na) \right] \right\} . \end{aligned} \quad (9)$$

## REFERENCES

1. C. W. Horton, Sr., Signal Processing of Underwater Acoustic Waves, (United States Government Printing Office, Washington, D.C., 1969).
2. H. Mermoz.: *Filtrage adapté et Utilisation Optimale d'une Antenne, Traitement du Signal avec Application Particulière à l'Acoustique Sous-marine*, Centre d'Étude des Phénomènes Aléatoires de Grenoble (CEPHAG), NATO Advanced Study Institute, Grenoble, France, 14-26 September 1964.
3. D. Middleton and H. L. Groginsky, "Detection of Random Acoustic Signals by Receivers with Distributed Elements: Optimum Receiver Structures for Normal Signal and Noise Fields," *J. Acoust. Soc. Am.* 38, 727-737 (1965).
4. T. D. Plemons, "Spectra, Covariance Functions, and Associated Statistics of Underwater Acoustic Scattering from Lake Surfaces," Dissertation, Department of Physics, The University of Texas at Austin, Austin, Texas, 1971. Also available as Applied Research Laboratories Technical Report No. 71-17 (ARL-TR-71-17).
5. T. D. Plemons, J. A. Shooter, and D. Middleton, "Underwater Acoustic Scattering from Lake Surfaces, I. Theory, Experiment, and Validation of the Data," *J. Acoust. Soc. Am.* 52, 1487-1502 (1972).
6. T. D. Plemons, J. A. Shooter, and D. Middleton, "Underwater Acoustic Scattering from Lake Surfaces, II. Covariance Functions and Related Statistics," *J. Acoust. Soc. Am.* 52, 1503-1515 (1972).
7. M. Frazer, "Some Statistical Properties of Lake Surface Reverberation," *J. Acoust. Soc. Am.* 64, 858-868 (1978).
8. M. Frazer, "A Study of the Properties of the Output of a Multidimensional Sonar Receiving Array Operating in a Reverberant Environment," Dissertation, Department of Physics, The University of Texas at Austin, Austin, Texas, June 1974. Also available as Applied Research Laboratories Technical Report No. 74-16 (ARL-TR-74-16).
9. Y. Omichi, "An Experimental Study of Covariance Functions of Reverberation from a Lake Surface," Thesis, College of Engineering, The University of Texas at Austin, Austin, Texas, May 1975. Also available as Applied Research Laboratories Technical Report No. 75-25 (ARL-TR-75-25).

10. J. Hoffman, "Target Classification Using Likelihood Ratios and Quadrature Components," Dissertation, Department of Physics, The University of Texas at Austin, Austin, Texas, June 1969. Also available as Applied Research Laboratories Technical Memorandum No. 69-11 (ARL-TM-69-11).
11. Jerome F. Hoffman, "Classification of Spherical Targets Using Likelihood Ratios and Quadrature Components," *J. Acoust. Soc. Am.* 41, 23-30 (1971).
12. C. R. Baker and R. F. Cunningham, "A Comparison of Detectors for Active Sonar Using Experimental Data" (U), Bendix Corp. Technical Report No. USWD-97-7, The Bendix Corporation, Electrodynamics Division, North Hollywood, California, March 1968. (CONFIDENTIAL)
13. H. L. Van Trees, Detection, Estimation, and Modulation Theory, Part I (John Wiley and Sons, Inc., New York, 1968).
14. E. L. Lehmann, Testing Statistical Hypotheses (John Wiley and Sons, Inc., New York, 1959).
15. H. Cramer, Mathematical Methods of Statistics (Princeton University Press, Princeton, New Jersey, 1971).
16. A. V. Oppenheim and R. W. Schafer, Digital Signal Processing (Prentice Hall, Inc., Englewood Cliffs, New Jersey, 1975).
17. O. D. Grace and S. P. Pitt, "Quadrature Sampling of High Frequency Waveforms," *J. Acoust. Soc. Am.* 44, 1453-1454(L), (1968).
18. O. D. Grace and S. P. Pitt, "Sampling and Interpolation of Bandlimited Signals by Quadrature Methods," *J. Acoust. Soc. Am.* 48, 1311-1318 (1970).
19. S. P. Pitt and O. D. Grace, "Signal Processing by Digital Quadrature Techniques," Applied Research Laboratories Technical Report No. 68-39 (ARL-TR-68-39), Applied Research Laboratories, The University of Texas at Austin, Austin, Texas, 30 December 1968.
20. R. Batey and B. Korts, "Lake Travis Test Station," Applied Research Laboratories, The University of Texas at Austin, Austin, Texas, 1973.
21. R. Barker, "Group Synchronization of Binary Digital Systems," in Communication Theory, W. Jackson (ed.) (Academic Press, New York and London, 1953) pp. 273-287.
22. "IMSL Library," Ed. 7, International Mathematical and Statistical Libraries, Inc., Houston, Texas (1979).
23. S. L. Adams and L. W. Nolte, "Bayes Optimum Array Detection of Targets of Known Location," *J. Acoust. Soc. Am.* 58, No. 3, 656-669 (1975).

24. R. B. Blackman and J. W. Tukey, The Measurement of Power Spectra  
(Dover Publications, Inc., New York, 1958).

3 March 1981

DISTRIBUTION LIST FOR  
ARL-TR-81-14  
UNDER CONTRACT N00014-80-C-0490  
UNCLASSIFIED

Copy No.

Commanding Officer  
Naval Ocean Research and Development Activity  
NSTL Station, MS 39529

1 Attn: A. L. Anderson (Code 320)  
2 J. A. Andrews (Code 300)  
3 E. Chaika (Code 530)  
4 R. Gardner (Code 520)  
5 R. R. Goodman (Code 110)  
6 H. Eppert (Code 360)  
7 S. Marshall (Code 340)  
8 L. Solomon (Code 500)

Commanding Officer  
Office of Naval Research  
Arlington, VA 22217

9 Attn: CAPT A. Gilmore (Code 200)  
10 G. R. Hamilton (Code 480)  
11 L. E. Hargrove (Code 421)  
12 J. McKisic (Code 486)  
13 R. Obrochta (Code 464)  
14 M. Odegard (Code 483)  
15 R. H. Register  
16 R. Ryan (Code 400R)  
17 E. I. Salkovitz (Code 400)  
18 CDR R. H. Schaus (Code 400B)  
19 J. A. Smith (Code 102)  
20 E. Wegman (Code 436)  
21 R. S. Winokur (Code 102C)

Commanding Officer  
Naval Electronic Systems Command  
Department of the Navy  
Washington, DC 20360

22 Attn: H. Ford (PME 124-60)  
23 J. Reeves (PME 124-30)  
24 J. Sinsky (Code 612)

Distribution List for ARL-TR-81-14 under Contract N00014-80-C-0490

(Cont'd)

Copy No.

Commander  
Naval Sea Systems Command  
Department of the Navy  
Washington, DC 20362  
25 Attn: R. Farwell (Code 63R)  
26 H. B. Latimer (Code 63)  
27 C. D. Smith (Code 63R)

Chief of Naval Material  
Office of Naval Technology  
Department of the Navy  
Washington, DC 20360  
28 Attn: CAPT E. Young

Commanding Officer  
Naval Oceanographic Office  
NSTL Station, MS 39529  
29 Attn: W. Geddes  
30 W. Jobst  
31 M. G. Lewis

Commander  
Naval Ocean Systems Center  
Department of the Navy  
San Diego, CA 92132  
32 Attn: Library  
33 N. O. Booth  
34 H. P. Bucker  
35 E. L. Hamilton  
36 M. A. Pedersen

Director  
Naval Research Laboratory  
Department of the Navy  
Washington, DC 20375  
37 Attn: R. Adams  
38 R. Mosley

Chief of Naval Operations  
Department of the Navy  
Washington, DC 20350  
39 Attn: CAPT J. Harlette (OP-952D1)

Distribution List for ARL-TR-81-14 under Contract N00014-80-C-0490

(Cont'd)

Copy No.

Commander  
Naval Air Development Center  
Department of the Navy  
Warminster, PA 18974  
Attn: C. L. Bartberger

40 Attn: C. L. Bartberger

Commander  
New London Laboratory  
Naval Underwater Systems Center  
Department of the Navy  
New London, CT 06320  
Attn: A. A. Filippini  
41  
42  
Library

41 Attn: A. A. Filippini  
42 Library

42 Library

46 B. Tolbe

### SUPERINTENDENT

Superintendent  
Newark Public School

Naval Postgraduate School  
Monterey, CA 93943-5000

Monterey, CA 93940

47 Attn: H. Medw

49 Woods Hole Oceanographic Institution  
50 Woods Hole, MA 02543  
51 Attn: E. Hayes  
52 C. Hollister  
53 B. Tucholke

Hawaii Institute of Geophysics  
The University of Hawaii  
2525 Correa Road  
Honolulu, HI 96822  
Attn: M. Manghnani  
G. Sutton

Distribution List for ARL-TR-81-14 under Contract N00014-80-C-0490 (Cont'd)

Copy No.

The Scripps Institution of Oceanography  
The University of California/San Diego  
San Diego, CA 92152  
54                   Attn: V. C. Anderson, Director  
                          Marine Physical Laboratory  
55                    F. Fisher  
56                    P. Lonsdale  
57                    R. Tyce

Department of Geological Oceanography  
Texas A&M University  
College Station, TX 77840  
58                   Attn: W. R. Bryant

Geophysics Laboratory  
Marine Science Institute  
The University of Texas  
700 The Strand  
Galveston, TX 77550  
59                   Attn: E. W. Behrens

The Catholic University of America  
6220 Michigan Avenue, NE  
Washington, DC 20017  
60                   Attn: H. M. Uberall

Lamont-Doherty Geological Observatory  
Palisades, NY 10964  
61                   Attn: G. Bryan  
62                    W. J. Ludwig  
63                    R. D. Stoll

Department of Civil and Ocean Engineering  
The University of Rhode Island  
Kinston, RI 02881  
64                   Attn: A. J. Silva

University College of North Wales  
Marine Science Laboratories  
Menai Bridge  
Anglesey, NORTH WALES  
65                   Attn: P. Schultheiss  
66                    D. Taylor Smith

Director  
SACLANT ASW Research Centre  
La Spezia, ITALY  
67                   Attn: T. Akal

AD-A100 507

TEXAS UNIV AT AUSTIN APPLIED RESEARCH LABS F/G 17/1  
AN EXPERIMENTAL INVESTIGATION OF A NEYMAN-PEARSON DETECTOR FOR --ETC(U)  
MAR 81 A J ESTES N00014-80-C-0490  
ARL-TR-81-14 NL

UNCLASSIFIED

20F2  
40  
3100360-7

END  
DATE  
FILED  
7-8-81  
DTIC

END  
DATE  
FILED  
7-8-1  
DTIC

Distribution List for ARL-TR-81-14 under Contract N00014-80-C-0490 (Cont'd)

Copy No.

68                   Department of Physics  
                  The University of Auckland  
                  Auckland, NEW ZEALAND  
                  Attn: A. Kibblewhite

69                   Defence Research Establishment Pacific  
                  CF Dockyard  
                  Victoria, B. C., CANADA B2Y 327  
                  Attn: Library

70                   Department of Civil Engineering  
                  The University of Texas at Austin  
                  Austin, TX 78712  
                  Attn: K. Stokoe

71-82               Commanding Officer and Director  
                  Defense Technical Information Center  
                  Cameron Station, Building 5  
                  5010 Duke Street  
                  Alexandria, VA 22314

83                   Southwest Research Institute  
                  P. O. Drawer 28510  
                  San Antonio, TX 78284  
                  Attn: T. Owen

84                   D. J. Shirley

85                   Electronics Research Laboratory  
                  The University of Trondheim  
                  The Norwegian Institute of Technology  
                  O. S. Bragstad Plass 6  
                  N-7034 Trondheim - NTH, NORWAY  
                  Attn: J. Hovem

86                   Department of Geology  
                  The University of Texas at Austin  
                  Austin, TX 78712  
                  Attn: M. Backus

87                   Office of Naval Research  
                  Branch Office Chicago  
                  Room 286, 536 South Clark Street  
                  Chicago, IL 60605

Distribution List for ARL-TR-81-14 under Contract N00014-80-C-0490 (Cont'd)

Copy No.

Applied Physics Laboratory  
University of Washington  
Seattle, WA 98105  
88 Attn: S. R. Murphy, Director

Applied Physics Laboratory  
The Johns Hopkins University  
Johns Hopkins Road  
Laurel, MD 20812  
89 Attn: J. Lombardo

Applied Research Laboratory  
The Pennsylvania State University  
P. O. Box 30  
State College, PA 16801  
90 Attn: John C. Johnson, Director

Office of Naval Research  
Resident Representative  
Room 582, Federal Building  
Austin, TX 78701  
91

Garland R. Barnard, ARL:UT  
92

David T. Blackstock, ARL:UT  
93

Raymond W. Bohls, ARL:UT  
94

Harlan G. Frey, ARL:UT  
95

Tom Griffy, ARL:UT  
96

Loyd Hampton, ARL:UT  
97

Robert E. Hollingsworth, ARL:UT  
98

Claude W. Horton, Sr., ARL:UT  
99

Chester M. McKinney, ARL:UT  
100

Stephen K. Mitchell, ARL:UT  
101

T. G. Muir, ARL:UT  
102

James M. Norwood, ARL:UT  
103

Tom Sager, ARL:UT  
104

Distribution List for ARL-TR-81-14 under Contract N00014-80-C-0490 (Cont'd)

Copy No.

105	Reuben H. Wallace, ARL:UT
106	Gary R. Wilson, ARL:UT
107	J. P. Woods, ARL:UT
108	Environmental Sciences Division, ARL:UT
109	Signal Physics Division, ARL:UT
110	Signal Physics Group, ARL:UT
111	Library, ARL:UT
112-123	Reserve, ARL:UT

